Automatika

Journal for Control, Measurement, Electronics, Computing and Communications

ISSN: (Print) (Online) Journal homepage: www.tandfonline.com/journals/taut20

Robust synchronization of four-dimensional chaotic finance systems with unknown parametric uncertainties

Muhammad Shafiq & Israr Ahmad

To cite this article: Muhammad Shafiq & Israr Ahmad (2024) Robust synchronization of four-dimensional chaotic finance systems with unknown parametric uncertainties, Automatika, 65:1, 217-234, DOI: 10.1080/00051144.2023.2295204

To link to this article: https://doi.org/10.1080/00051144.2023.2295204

Published online: 27 Dec 2023.

AUTOMATIKA
2023, VOL. 65, NO. 1, 217–234
https://doi.org/10.1080/00051144.2023.2295204

Robust synchronization of four-dimensional chaotic finance systems with unknown parametric uncertainties

Muhammad Shafiq[a] and Israr Ahmad [b]

[a]Department of Electrical and Computer Engineering, Sultan Qaboos University Muscat, Oman; [b]Department of Information Technology, University of Technology and Applied Sciences Nizwa, Nizwa, Oman

ABSTRACT

The inherent randomness in economic factors causes complex and irregular behaviour that affects financial system stability and economic growth. Such chaotic behaviour can make it difficult to synchronize financial systems. The chaotic finance system synchronization precision maintains financial stability and economic growth. In this paper, the controller design procedure assumes that the financial system is exposed to unknown bounded exogenous disturbances and model uncertainties. This research proposes a novel direct adaptive control strategy that achieves robust synchronization of two identical four-dimensional finance chaotic (FDFC) systems. The proposed controller establishes a faster, smoother synchronization error vector convergence to zero. The controller design procedure does not eliminate the closed-loop's nonlinear terms and is independent of the financial system parameters. These controller's attributes accomplish the closed-loop robust performance. Further, this controller uses real-time estimates of unknown model uncertainties and bounds to compensate for unknown exogenous disturbances. Computer simulation results and proofs of theoretical analysis based on the Lyapunov stability theory confirm that the proposed control technique compels the error vector trajectories to the origin in a short transient time with less active oscillations for all signals. The paper includes comparative computer simulations for verifying the theoretical findings.

ARTICLE HISTORY
Received 7 September 2022
Accepted 6 December 2023

KEYWORDS
Hyperchaotic finance system; Lyapunov stability theory; adaptive controller; chaos synchronization

1. Introduction

Chaotic dynamical systems show sensitivity to variations in the parameters and initial conditions; such systems display irregular, unpredictable, and complex behaviour [1]. Several nonlinear dynamical systems in social and natural sciences exhibit chaos [1,2].

The intrinsic random nature of economic factors originates complex and irregular behaviour in a time-varying uncertain nonlinear finance system [3]. Stock market price's abrupt variations, environmental interferences, exchange rate fluctuations, and interest rate alteration due to external forces, among other economic factors, change the savings amount in a financial system; the periodic dynamics of the financial system transform into chaos [4–6]. Chaos in financial and economic systems concedes that the uncertainties in the macroeconomic operations produce disturbances that lead to financial system crises [5]. The chaotic nature of the financial systems affects short-medium-long-term economic planning and predictions [6].

The chaotic synchronization of finance dynamical systems has been an active research area for the last two decades. It has produced numerous feedback controller schemes for synchronizing the financial system's chaotic behaviour. A brief literature review of this research is as follows. The paper [7] realizes the synchronization of two coupled three-dimensional chaotic finance (TDCF) systems. The closed-loop stability is investigated using the Routh-Hurwitz criterion when the finance system's parameters are known and active adaptive feedback controller for uncertain parameters. The article [8] derives a nonlinear adaptive-impulsive control strategy and employs the impulsive dynamical systems' invariant principle for synchronizing two identical four-dimensional finance chaotic (FDFC) systems. A set of sufficient conditions for impulsive synchronization using a comparative approach for impulsive functional differential equations is derived, and upper bounds for the impulsive interval necessary for stable synchronization are estimated. The article [9] discusses the robust chaotic synchronization of two uncertain FDFC systems with bounded exogenous disturbances. The authors [10] propose a time-varying delay nonlinear adaptive control technique for synchronizing two identical TDCF systems with exogenous disturbances. The paper [11] discusses the two mixed synchronization strategies for two identical TDFC systems and compares the closed loops using simulation results. Utilizing the Lyapunov stability theory, the paper [12] uses the adaptive control algorithm for synchronizing two identical uncertain FDFC systems. The authors [13] employ the

CONTACT Israr Ahmad iak_2000plus@yahoo.com University of Technology and Applied Sciences Nizwa, Ministry of Higher Education, Postal Code: 611, Post Box: 699, Nizwa, Sultanate of Oman

linear feedback control technique to synchronize two identical TDFC systems. Ref. [14] investigates the network synchronization of many uncertain FDFC systems by estimating uncertain system parameters. The network synchronization is achieved by calculating the Lyapunov exponent of the network. The article [15] investigates the FDFC system synchronization using a conventional nonlinear control method. The authors [16] propose an adaptive control strategy for synchronizing two identical FDFC systems by estimating uncertain system parameters. Based on the Lyapunov stability theory, sufficient conditions are derived, and a linear feedback control technique is designed [17] for the global asymptotic synchronization of two identical FDFC systems. Ref. [18] achieves fixed-time synchronization of two identical FDFC systems using the drive-response system arrangement.

The following items discuss the motivations and challenges.

(1) The feedback control strategies [7–16,18] synchronizing two identical TDCF/FDFC systems follow the nonlinear terms cancellation approach. These strategies need the exact measurement of the state variables and parameters. However, the state variable's precise measurement offers complications due to the noise and parameter uncertainties in the measurement system and plant dynamics. Consequently, residual nonlinear terms contaminate the closed loops developed using such controller design approaches [7–16,18]. Hence, these controller methodologies assimilate erroneous control efforts, possibly causing instability in the closed-loop system. Moreover, these residual terms disturb the closed-loop performance, including transient behaviour and steady-state that produce long-time delays.
(2) Reducing energy consumption in the synchronization process is a challenging problem. Oscillation-free error convergence consumes low energy; it motivates the development of less oscillatory fast convergence synchronization controllers. The accuracy of the synchronization of two coupled finance chaotic systems maintains financial stability and economic growth. The control efforts computed by the feedback controllers proposed in [7–18] consume high energy to realize synchronization behaviour, resulting in large fluctuations in the synchronization errors and control signals [7–18]; it causes adverse effects that lead to economic crises; the financial system may lose complete economic stability in the worst-case scenario. The FDCF systems synchronization precision is essential for maintaining financial stability and economic growth.
(3) The financial systems are exposed to certain exogenous disturbances due to environmental interference [19]; it depends on the investment demand and time in practice. These disturbances generate undesirable behaviour and increase the uncertainty that disrupts market functioning, introduce systemic risks that affect economic growth and destabilize the financial system leading to economic crises [20]. The proposed controller approaches [7,8,10–18] do not consider the effect of the time-varying model uncertainties and exogenous disturbances.
(4) Controllers in [7–18] can furnish a smaller synchronization error convergence gradient; it may increase vulnerability and can cause prolonged instability and investor uncertainty.

The abovementioned challenges motivate a state-feedback controller design that synchronizes two identical FDFC systems; developing a closed-loop structure should possess the following attributes.

(1) The controller should avoid the closed-loop's nonlinear terms cancellation.
(2) It should reduce the state error vector trajectories and control signal oscillations.
(3) It should show robustness to time-varying unknown model uncertainties and exogenous disturbances.
(4) It should achieve faster error vector convergence rates in the origin's direction.

This article aims to achieve two key objectives regarding controller design procedure.

(1) Development of the robust closed-loop
The proposed closed-loop should be insensitive to exogenous disturbances, and parameter variations should be smooth and slow. The closed-loop system's insensitivity to parameter variations and exogenous disturbances enhances feedback controllers' robustness and improves system performance, fault tolerance, and adaptability. These features allow the system to operate reliably and effectively within changing conditions and uncertainties.
(2) Synthesizing a smooth control effort
The controller should synthesize a smooth control effort to make the closed-loop energy efficient. Smooth control effort does not produce fluctuations in the closed-loop dynamical system; it keeps the synchronization stability of financial systems and operates a smooth, healthy economic cycle.

Therefore, this article proposes a novel robust direct adaptive synchronization control strategy (RDASCS) that resolves the aforementioned issues. The proposed controller in this paper for synchronizing two identical FDFC systems is a novel design. The article also devises an analytical procedure for studying closed-loop stability.

The closed-loop formed by incorporating the proposed adaptive synchronization control algorithm characteristics are as follows.

(1) It develops a faster oscillation-free stable closed-loop: it reduces risks, improves data accuracy, and enhances stability and processing capabilities for time-sensitive transactions.
(2) The control input to the nonlinear control system does not depend on the system's nonlinear terms; this makes the closed-loop stability performance independent of the time-varying model uncertainties and exogenous disturbances. This controller attribute flourishes robust closed-loop stability, makes the system more predictable, and simplifies the controller design and analysis processes.
(3) The control signals are less oscillatory and chatter-free; such control efforts do not develop fluctuations in the financial system dynamics and economic growth operations. This feature of the controller design makes the control effort variations smoother against uncertainties or environmental changes.

The proposed algorithm improves financial system stability by reducing the unanticipated fluctuations and crashes risk. Benefits of the less active synchronization oscillations include increased efficiency and productivity and decreased investment demands.

The article provides a detailed stability analysis utilizing the Lyapunov second theorem of stability [21], ensuring a robust, asymptotic stable closed-loop. The paper discusses the computer-based simulation results verifying the theoretical findings. The article compares the closed-loop's performance with other state-of-the-art synchronization control methodologies [13,22] using computer-based simulation results.

The breakdown of the remaining papers' structure is as follows.

Section 2 provides the relevant terminology. In Section 3, the article illustrates the four-dimensional finance chaotic system dynamics. Section 4 discusses the synchronization problem between two identical four-dimensional chaotic finance systems with unknown parametric uncertainties. Section 5 designs a novel feedback controller for synchronizing two identical four-dimensional chaotic systems in the master-slave system arrangement and provides proof of robust closed-loop stability. Section 6 gives numerical simulations with a comparative study. The article concludes in Section 7.

2. Notations and symbols

Table 1 describes the terminology.

3. Dynamics of the four-dimensional chaotic finance model

The authors [3] proposed a three-dimensional finance chaotic (TDFC) system. The TDFC system consists of four sub-components: labour force, production, stock, and money. The TDFC dynamics system in matrix form is given in Equation (1).

$$\dot{\mathbf{x}}(t) = \begin{bmatrix} -a_1 & 0 & 1 \\ 0 & -a_2 & 0 \\ -1 & 0 & -a_3 \end{bmatrix} \begin{bmatrix} x_1(t) \\ x_2(t) \\ x_3(t) \end{bmatrix} + \begin{bmatrix} 0 \\ 1 \\ 0 \end{bmatrix} + \begin{bmatrix} x_1(t)x_2(t) \\ -x_1^2(t) \\ 0 \end{bmatrix} \tag{1}$$

where $x_1(t)$, $x_2(t)$, and $x_3(t)$ are the state variables representing the rate of interest, investment demand, and price index, alternatively [3]. The state variable $x_1(t)$ is influenced by the goods price structural adjustment and investment market contradiction. The rate of change of state variable $x_2(t)$ is related to the investment and interest rates and cost investment inversion. The state variable $x_3(t)$ depends on inflation rates, the contradiction between the commercial market supply and demand also controls it [3]. The parameters $a_1 > 0$, $a_2 > 0$, and $a_3 > 0$ denote the saving amount, investment cost, and commercial markets elasticity demand, alternatively.

The research article [6] introduces a new state variable $x_4(t)$ to the TDFC system (1) that represents the average profit margin and proposes the dynamics of an FDFC system. Hence, Equation (2) describes the new FDFC system's dynamics in vector form.

$$\dot{\mathbf{x}}(t) = \begin{bmatrix} -a_1 & 0 & 1 & 1 \\ 0 & -a_2 & 0 & 0 \\ -1 & 0 & -a_3 & 0 \\ 0 & 0 & 0 & -a_4 \end{bmatrix} \begin{bmatrix} x_1(t) \\ x_2(t) \\ x_3(t) \\ x_4(t) \end{bmatrix} + \begin{bmatrix} x_1(t)x_2(t) \\ -x_1^2(t) \\ 0 \\ -a_5x_1(t)x_2(t) \end{bmatrix} + \begin{bmatrix} 0 \\ 1 \\ 0 \\ 0 \end{bmatrix} \tag{2}$$

where $a_4 > 0$ and $a_5 > 0$ are the constant parameters [6].

The following section comprises five fundamental system characteristics that describe chaos in the finance system (2).

Table 1. Nomenclature.

Symbols	Description
x and **X**	**x** denotes an $n \times 1$ vector, and **X** represents an $n \times n$ matrix
R	Real numbers
T	Transpose of a vector/matrix
MSS	Master-Slave system
$\mathrm{x}(t) = \begin{bmatrix} x_1(t) & x_2(t) & x_3(t) & x_4(t) \end{bmatrix}^T \in R^{4\times 1}$	FDFC system's (2) state variables vector
a_1, a_2, a_3, a_4, and a_5	FDFC system's (2) constant parameters
$\mathrm{x}^m(t) = \begin{bmatrix} x_1^m(t) & x_2^m(t) & x_3^m(t) & x_4^m(t) \end{bmatrix}^T \in R^{4\times 1}$, and $\mathrm{x}^s(t) = \begin{bmatrix} x_1^s(t) & x_2^s(t) & x_3^s(t) & x_4^s(t) \end{bmatrix}^T \in R^{4\times 1}$	MSS (10–11) state variables vectors
$\mathrm{e}(t) = \mathrm{x}^s(t) - \mathrm{x}^m(t) = \begin{bmatrix} e_1(t) & e_2(t) & e_3(t) & e_4(t) \end{bmatrix}^T \in R^{4\times 1}$	MSS (10–11) synchronization error vector
$\boldsymbol{\gamma}^m(\mathrm{x}^m(t)) = \begin{bmatrix} \gamma_1^m(x_1^m(t)) & \gamma_2^m(x_2^m(t)) & \gamma_3^m(x_3^m(t)) & \gamma_4^m(x_4^m(t)) \end{bmatrix}^T \in R^{4\times 1}$, and $\boldsymbol{\gamma}^m(\mathrm{x}^s(t)) = \begin{bmatrix} \gamma_1^s(x_1^s(t)) & \gamma_2^s(x_2^s(t)) & \gamma_3^s(x_3^s(t)) & \gamma_4^s(x_4^s(t)) \end{bmatrix}^T \in R^{4\times 1}$	Vectors of the unknown time-varying model uncertainties present in the MSS (10–11), respectively
$\boldsymbol{\gamma}^m = \begin{bmatrix} \gamma_1^m & \gamma_2^m & \gamma_3^m & \gamma_4^m \end{bmatrix}^T \in R^{4\times 1}$, $\boldsymbol{\gamma}^s = \begin{bmatrix} \gamma_1^s & \gamma_2^s & \gamma_3^s & \gamma_4^s \end{bmatrix}^T \in R^{4\times 1}$, and $\boldsymbol{\gamma}^m + \boldsymbol{\gamma}^s = \boldsymbol{\gamma} = \begin{bmatrix} \gamma_1 & \gamma_2 & \gamma_3 & \gamma_4 \end{bmatrix}^T \in R^{4\times 1}$	$\boldsymbol{\gamma}^m$ and $\boldsymbol{\gamma}^s$ are the vectors that represent the least upper bounds of $\boldsymbol{\gamma}^m(\mathrm{x}^m(t))$ and $\boldsymbol{\gamma}^s(\mathrm{x}^s(t))$, respectively
$\boldsymbol{\delta}^m(t) = \begin{bmatrix} \delta_1^m(t) & \delta_2^m(t) & \delta_3^m(t) & \delta_4^m(t) \end{bmatrix}^T \in R^{4\times 1}$, and $\boldsymbol{\delta}^s(t) = \begin{bmatrix} \delta_1^s(t) & \delta_2^s(t) & \delta_3^s(t) & \delta_4^s(t) \end{bmatrix}^T \in R^{4\times 1}$	Vectors of the unknown time-varying exogenous disturbances acting on the MSS (10–11), respectively
$\boldsymbol{\delta}^m = \begin{bmatrix} \delta_1^m & \delta_2^m & \delta_3^m & \delta_4^m \end{bmatrix}^T \in R^{4\times 1}$, $\boldsymbol{\delta}^s = \begin{bmatrix} \delta_1^s & \delta_2^s & \delta_3^s & \delta_4^s \end{bmatrix}^T \in R^{4\times 1}$, and $\boldsymbol{\delta}^m + \boldsymbol{\delta}^s = \boldsymbol{\delta} = \begin{bmatrix} \delta_1 & \delta_2 & \delta_3 & \delta_4 \end{bmatrix}^T \in R^{4\times 1}$	$\boldsymbol{\delta}^m$ and $\boldsymbol{\delta}^s$ are the vectors that represent the least upper bounds of $\boldsymbol{\delta}^m(t)$ and $\boldsymbol{\delta}^s(t)$, respectively
$\mathrm{u}(t) = \begin{bmatrix} u_1(t) & u_2(t) & u_3(t) & u_4(t) \end{bmatrix}^T$	Control input vector
$\mathrm{K} = \{k_{ij}, i \neq j \Rightarrow k_{ij} = 0\} \in R^{4\times 4}$, and $\boldsymbol{\psi} = \{\psi_{ij}, i \neq j \Rightarrow \psi_{ij} = 0\} \in R^{4\times 4}$ for $i, j = 1, 2, 3, 4$	The feedback controller gains matrices
ϱ, ρ, φ	Controller parameters
e	Logarithmic base
σ	Positive real constant
$\hat{\boldsymbol{\gamma}}(t) = \begin{bmatrix} \hat{\gamma}_1(t) & \hat{\gamma}_2(t) & \hat{\gamma}_3(t) & \hat{\gamma}_4(t) \end{bmatrix} \in R^{4\times 1}$, and $\hat{\boldsymbol{\delta}}(t) = \begin{bmatrix} \hat{\delta}_1(t) & \hat{\delta}_2(t) & \hat{\delta}_3(t) & \hat{\delta}_4(t) \end{bmatrix} \in R^{4\times 1}$	Parameters of the controller (16), which are unknown
$\circ$	Hadamard operator
$\dot{V}(t)$	The time derivative of $V(t)$
$\lvert x \rvert$	Scalar absolute, where $x \in R$
$\lvert \mathrm{x} \rvert = [\lvert x_1 \rvert, \lvert x_2 \rvert, \ldots, \lvert x_n \rvert]^T$	Vector absolute, where $\mathrm{x} \in R^{n\times 1}$ and $x_i \in \mathrm{x}, i = 1, 2, \cdots, n$
$\lVert \lvert \mathrm{x}_1 \rvert \rVert = \sum_1^n \lvert x_i \rvert$	$\mathcal{L}_1$ of x

3.1. Balancing points stability analysis

Balancing points stability analysis studies the system's state variable trajectory behaviour established due to steady-state disturbances. $\dot{x}_i(t) = \dot{x}_2(t) = \dot{x}_3(t) = \dot{x}_4(t) = 0$ shows the steady state of system (2). Therefore,

$$\begin{cases} x_1(t)(x_2(t) - a_1) + x_3(t) + x_4(t) = 0 \\ 1 - a_2 x_2(t) - x_1^2(t) = 0 \\ -a_3 x_3(t) - x_1(t) = 0 \\ -a_4 x_4(t) - a_5 x_1(t) x_2(t) = 0 \end{cases} \tag{3}$$

Equation (4) describes the balancing points of system (2), when $\frac{a_2 a_5 + a_3 a_4 + a_1 a_2 a_3 a_5 - a_3 a_5}{a_3(a_4 - a_5)} > 0$.

$$\begin{aligned} x_{e1} &= \left[0, \frac{1}{a_2}, 0, 0\right], \\ x_{e2,3} &= \left[\pm\vartheta, \left(\frac{a_1 a_3 a_5}{a_3(a_5 - a_4)}\right), \right. \\ &\quad \left. \mp \frac{\vartheta}{a_3}, \left(\frac{a_4 \vartheta (1 + a_1 a_3)}{a_3(a_4 - a_5)}\right)\right], \end{aligned} \tag{4}$$

where $\vartheta = \sqrt{1 + \frac{a_2 a_5 + a_1 a_2 a_3 a_5}{a_3(a_4 - a_5)}}$.

The Jacobean matrix of system (2) is given below.

$$J_{x(t)} = \begin{bmatrix} -a_1 + x_2(t) & x_1(t) & 1 & 1 \\ -2x_1(t) & -a_2 & 0 & 0 \\ -1 & 0 & -a_3 & 0 \\ -a_5 x_2(t) & -a_5 x_1(t) & 0 & -a_4 \end{bmatrix}. \tag{5}$$

The computer simulation results in this article consider $a_1 = 0.9, a_2 = 0.2, a_3 = 1.2, a_4 = 0.17$, and $a_5 = 0.2$ [6] with initial conditions $[x_1(t)\ x_2(t)\ x_3(t)\ x_4(t)]^T = [0.1\ 0.3\ 0.5\ 0.2]^T$. Analysis in Table 2 shows that all the balancing points are saddle-focus, determining that the finance system (2) exhibits chaos.

3.2. Dissipative behaviour

The presence of a strange attractor in a nonlinear dynamical system guarantees chaos in the system [23]. The negative vector field's divergence assures a dissipative system.

Following (2), let us consider the vector field **v** as follows.

$$\mathbf{v} = \begin{bmatrix} \dot{x}_1(t) \\ \dot{x}_2(t) \\ \dot{x}_3(t) \\ \dot{x}_3(t) \end{bmatrix} = \begin{bmatrix} (x_2(t) - a_1)x_1(t) + x_3(t) + x_4(t) \\ 1 - a_2 x_2(t) - x_1^2(t) \\ -a_3 x_3(t) - x_1(t) \\ -a_4 x_4(t) - a_5 x_1(t) x_2(t) \end{bmatrix}. \tag{6}$$

Table 2. The FDFC system (2) stability analysis.

i	x_{ei}	$\lambda_{ij}, i,j = 1,2,3,4$	Stability analysis
1	x_{e1}	$\lambda_{11} = 3.62978,\ \lambda_{12} = 0.141217,\ \lambda_{13} = -0.2,\ \lambda_{14} = -1.04099$	x_{e1} shows an unstable (saddle-focus) balancing point
2	x_{e2}	$\lambda_{21} = -11.3412,\ \lambda_{22} = -1.2558, \lambda_{23} = 0.24306,\ \lambda_{24} = 0.06166$	x_{e2} shows an unstable (saddle-focus) balancing point
3	x_{e3}	$\lambda_{31} = 9.2326,\ \lambda_{32} = 0.04068, \lambda_{33,34} = -0.961 \pm 0.1491i$	x_{e3} shows an unstable (saddle-focus) balancing point

Equation (7) gives the divergence.

$$\begin{aligned}\nabla.\mathbf{v} = &\frac{\partial((x_2(t)-0.9)x_1(t)+x_3(t)+x_4(t))}{\partial x_1(t)}\\ &+\frac{\partial(1-0.2x_2(t)-x_1^2(t))}{\partial x_2(t)}\\ &+\frac{\partial(-1.2x_3(t)-x_1(t))}{\partial x_3(t)}\\ &+\frac{\partial(-0.17x_4(t)-0.2x_1(t)x_2(t))}{\partial x_4(t)}\\ &= x_2(t)-0.9-0.2-1.2-0.17 = x_2(t)-2.47.\end{aligned} \tag{7}$$

The dynamical system (2) is dissipative for $x_2(t) < 2.47$. It means that for each vector element $\mathbf{v}_0 e^{-(x_2(t)-2.47)t}$ that contains trajectories of system (2) converge to zero exponentially with a rate of $(x_2(t) - 2.47)$ as $t \to \infty$. Consequently, the dynamic model (2) state trajectories are attracted by a strange attractor; therefore, the four-dimensional financial system (2) exhibits chaos [23].

3.3. Lyapunov exponents and lyapunov dimension

The two nearby trajectories diverge at a time zero, and the distance between them grows exponentially. The Lyapunov exponents (LE) measure sensitive dependence on initial conditions at $t = 0$ [24]; it is calculated based on how rapidly two nearby states diverge. The LE of the financial system (2) are $LE_1 = 0.034432$, $LE_2 = 0.018041$, $LE_3 = 0.00$, and $LE_4 = -1.1499$.

Now,

$$\begin{aligned}&0.034432 + 0.018041 + 0.00 - 1.1499\\ &= -0.097427 < 0.\end{aligned} \tag{8}$$

Therefore, the four-dimensional finance system (2) is chaotic [24].

Equation (9) computes the Lyapunov dimension (L_D) of system (2).

$$\begin{aligned}L_D &= j + \frac{\sum_{i=1}^{j} LE_j}{|LE_{j+1}|} = 3 + \frac{0.034432 + 0.018041}{1.1449}\\ &= 3.050121,\end{aligned} \tag{9}$$

which is fractional. Equations (8–9) confirm chaos in the finance system (2) [24].

3.4. Poincare sections

This subsection discusses the continuous dynamical system's long-term stability based on the Poincare sections (maps) analysis. This procedure transforms the continuous dynamical system into a discrete state-space system having one dimension less than the original system [25]. Fractals in the state-variable trajectories behaviour on a Poincare section indicate chaos in the dynamical system. Figure 4(a–d) illustrates the Poincare maps of system (2).

3.5. Bifurcation graphs

The qualitative shifts in the dynamical system vector fields caused by the plant parameter variations are known as bifurcation. The values of the parameters where such qualitative changes occur are called bifurcation values [25]. Figure 5(a–d) shows the bifurcation plots for the variations in the system parameter $a_3 \in [0, 2.5]$ verses state variables $x_i(t)$, $i = 1, 2, 3, 4$. These figures confirm that the four-dimensional finance system (2) is chaotic.

The finance system (2) exhibits chaos for the values of parameters $a_1 = 0.9$, $a_2 = 0.2$, $a_3 = 1.5$, $a_4 = 0.17$, and $a_5 = 0.2$. The 3D and 2D chaotic attractors are shown in Figures 1 and 2(a–f). Figure 3(a-d) depicts the state variable trajectories' behaviour. Figures 4 and 5(a–d) show Poincare maps and bifurcation graphs, respectively.

The following section formulates the problem of synchronizing two identical FDFC systems described in (2).

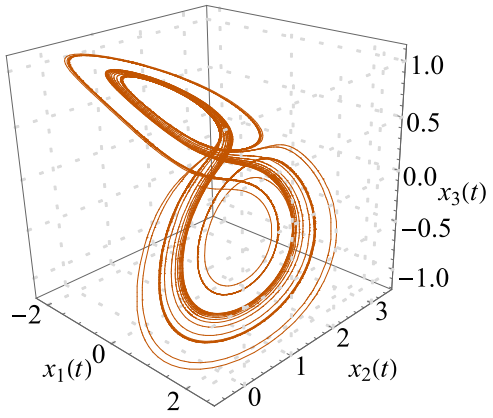

Figure 1. 3-D chaotic attractor of the FDFC system (2).

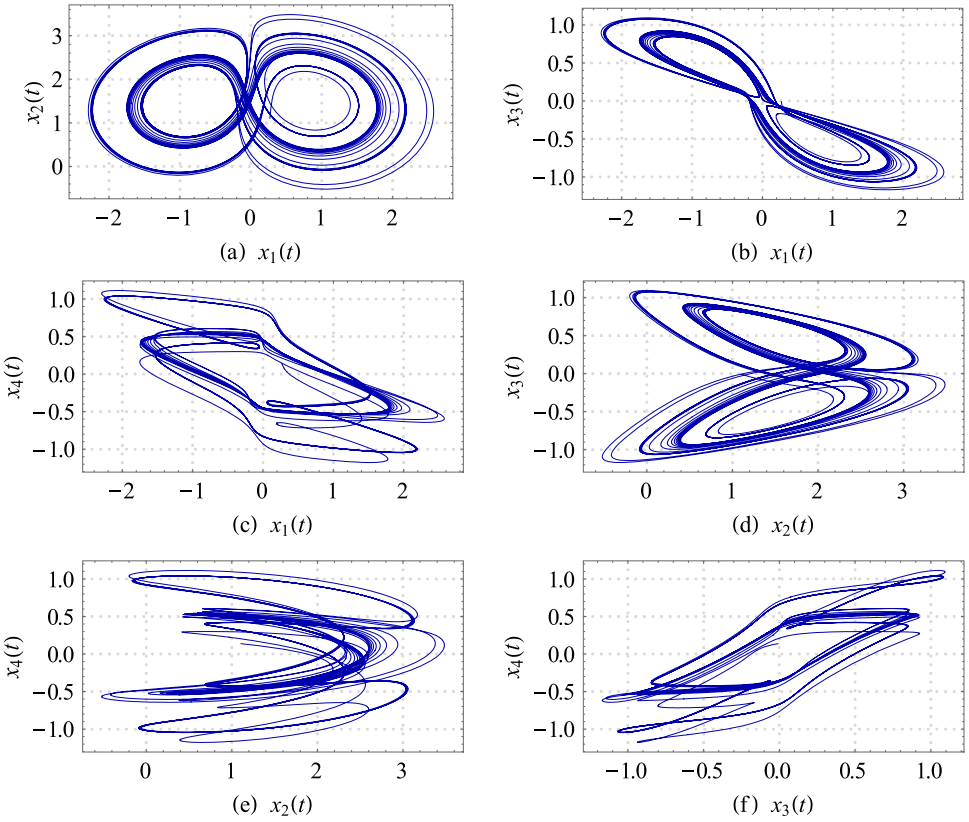

Figure 2. (a) $x_1(t)$ and $x_2(t)$ projection, (b) $x_1(t)$ and $x_3(t)$ projection, (c) $x_1(t)$ and $x_4(t)$ projection, (d) $x_2(t)$ and $x_3(t)$ projection, (e) $x_2(t)$ and $x_4(t)$ projection, and (f) $x_3(t)$ and $x_4(t)$ projection.

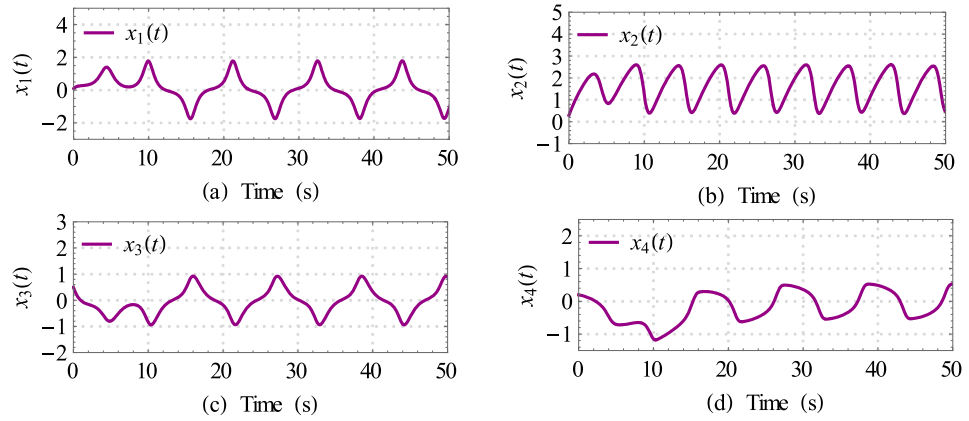

Figure 3. The state variable trajectories behaviour, (a) $x_1(t)$, (b) $x_2(t)$, (c) $x_3(t)$, and (d) $x_4(t)$.

4. Problem formulation

4.1. Synchronization between two identical FDFC systems with unknown parametric uncertainties

Let $\mathbf{x}^m(t)$ and $\mathbf{x}^s(t)$ are the state variables vectors of master and slave FDFC systems, respectively. Equations (10 and 11) give the MSS configuration for the FDFC system (2) and $\mathbf{u}(t) \in R^{4\times 1}$ is a control input vector for synchronizing the slave FDFC system (11) with the master system (10). Further, $\boldsymbol{\delta}^m(t)$ and $\boldsymbol{\delta}^s(t)$ represent vectors of the time-varying unknown bounded exogenous disturbances, and $\boldsymbol{\gamma}^m(\mathbf{x}^m(t))$ and $\boldsymbol{\gamma}^s(\mathbf{x}^s(t))$ denote vectors of the time-varying unknown bounded model uncertainties.

Master FDFC System:

$$\dot{\mathbf{x}}^m(t) = \begin{bmatrix} -a_1 & 0 & 1 & 1 \\ 0 & -a_2 & 0 & 0 \\ -1 & 0 & -a_3 & 0 \\ 0 & 0 & 0 & -a_4 \end{bmatrix} \begin{bmatrix} x_1^m(t) \\ x_2^m(t) \\ x_3^m(t) \\ x_4^m(t) \end{bmatrix} + \begin{bmatrix} x_1^m(t)x_2^m(t) \\ -(x_1^2(t))^m \\ 0 \\ -a_5 x_1^m(t)x_2^m(t) \end{bmatrix} + \begin{bmatrix} 0 \\ 1 \\ 0 \\ 0 \end{bmatrix} + \boldsymbol{\gamma}^m(\mathbf{x}^m(t)) + \boldsymbol{\delta}^m(t) \tag{10}$$

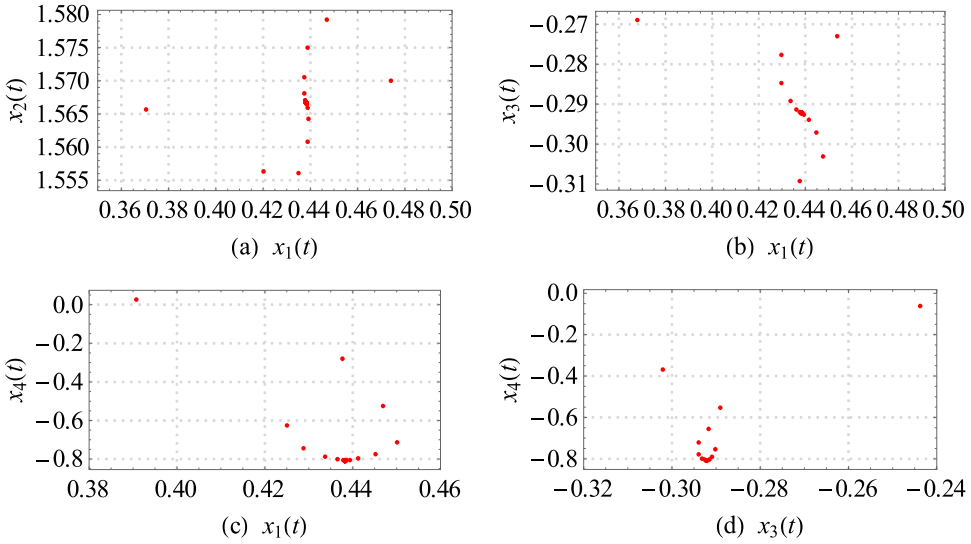

Figure 4. Poincare sections, (a) $x_1(t)vs\,x_2(t)$, (b) $x_1(t)vs\,x_3(t)$, (c) $x_1(t)vs\,x_4(t)$, and (d) $x_3(t)vs\,x_4(t)$.

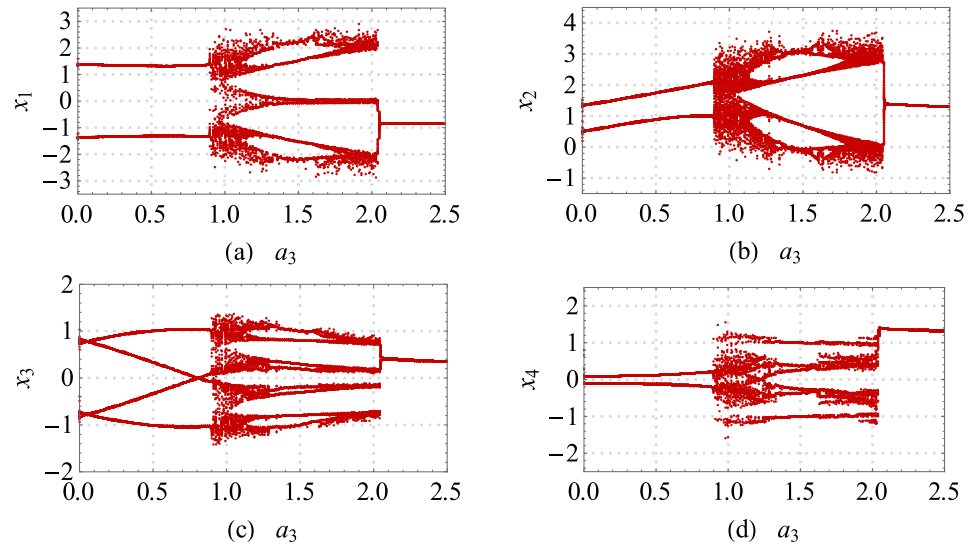

Figure 5. Bifurcation graphs, (a) a_3vsx_1, (b) a_3vsx_2, (c) a_3vsx_3, (d) a_3vsx_4.

Slave FDFC system:

$$\dot{\mathbf{x}}^s(t) = \begin{bmatrix} -a_1 & 0 & 1 & 1 \\ 0 & -a_2 & 0 & 0 \\ -1 & 0 & -a_3 & 0 \\ 0 & 0 & 0 & -a_4 \end{bmatrix} \begin{bmatrix} x_1^s(t) \\ x_2^s(t) \\ x_3^s(t) \\ x_4^s(t) \end{bmatrix} + \begin{bmatrix} x_1^s(t)x_2^s(t) \\ -(x_1^2(t))^s \\ 0 \\ -a_5 x_1^s(t)x_2^s(t) \end{bmatrix} + \begin{bmatrix} 0 \\ 1 \\ 0 \\ 0 \end{bmatrix} + \boldsymbol{\gamma}^s(\mathbf{x}^s(t)) + \boldsymbol{\delta}^s(t) + \mathbf{u}(t). \tag{11}$$

Equation (12) describes the synchronization error dynamics of the MSS (10–11).

$$\dot{\mathbf{e}}(t) = \begin{bmatrix} -a_1 & 0 & 1 & 1 \\ 0 & -a_2 & 0 & 0 \\ -1 & 0 & -a_3 & 0 \\ 0 & 0 & 0 & -a_4 \end{bmatrix} \mathbf{e}(t) + \begin{bmatrix} x_2^s(t)e_1(t) + x_1^m(t)e_2(t) \\ -e_1(t)(x_1^m(t) + x_1^s(t)) \\ 0 \\ -a_5(x_2^s(t)e_1(t) + x_1^m(t)e_2(t)) \end{bmatrix} + \boldsymbol{\gamma}^{ms}(\mathbf{x}^{ms}(t)) + \boldsymbol{\delta}^{ms}(t) + \mathbf{u}(t), \tag{12}$$

where

$$\begin{cases} \dot{\mathbf{e}}(t) = \dot{\mathbf{x}}^s(t) - \dot{\mathbf{x}}^m(t), \\ x_1^s(t)x_2^s(t) - x_1^m(t)x_2^m(t) = x_2^s(t)e_1(t) + x_1^m(t)e_2(t) \\ (x_1^2(t))^m - (x_1^2(t))^s = -e_1(t)(x_1^m(t) + x_1^s(t)), \\ \boldsymbol{\gamma}^{ms}(\mathbf{x}^{ms}(t)) := \boldsymbol{\gamma}^s(\mathbf{x}^s(t)) - \boldsymbol{\gamma}^m(\mathbf{x}^m(t)), \\ \boldsymbol{\delta}^{ms}(t) := \boldsymbol{\delta}^s(t) - \boldsymbol{\delta}^m(t). \end{cases} \tag{13}$$

Assumption 4.1: *The speculative behaviour creates fluctuations in the market that produce uncertainties in financial systems; it gives birth to economic crises in the financial system* [19]. *The financial systems are also*

exposed to certain disturbances [20]. *Let us assume the unknown model uncertainties* $\{\boldsymbol{\gamma}(\boldsymbol{x}^m(t)), \boldsymbol{\gamma}(\boldsymbol{x}^s(t))\}$ *and exogenous disturbances* $\{\boldsymbol{\delta}^m(t), \boldsymbol{\delta}^s(t)\}$ *are bounded, and Equations* (14) *and* (15) *define their bounds, respectively.*

$$|\gamma_i(x_i^m(t))| \leq \gamma_i^m,\ |\gamma_i(x_i^s(t))| \leq \gamma_i^s,\ i = 1,2,3,4.$$
$$\Rightarrow$$
$$\begin{aligned}|\gamma_i(x_i^s(t)) - \gamma_i(x_i^m(t))| &\leq |\gamma_i(x_i^s(t)) + \gamma_i(x_i^m(t))| \\ &\leq |\gamma_i(x_i^s(t))| \leq |\gamma_i(x_i^m(t))| \leq \gamma_i^s + \gamma_i^m \leq \gamma_i, \\ i &= 1,2,3,4, \end{aligned} \tag{14}$$

and

$$|\delta_i^m(t)| \leq \delta_i^m,\ |\delta_i^s(t)| \leq \delta_i^s,\ i = 1,2,3,4.$$
$$\Rightarrow$$
$$\begin{aligned}|\delta_i^s(t) - \delta_i^m(t)| &\leq |\delta_i^s(t) + \delta_i^m(t)| \\ &\leq |\delta_i^s(t)| + |\delta_i^s(t) + \delta_i^m(t)| \leq \delta_i^s + \delta_i^m \leq \delta_i, \\ i &= 1,2,3,4. \end{aligned} \tag{15}$$

Hence, Equaitons (14) and (15) conclude that:

$$\begin{aligned}&|\gamma_i(x_i^s(t)) - \gamma_i(x_i^m(t)) + \delta_i^s(t) - \delta_i^m(t)| \\ &\quad \leq |\gamma_i(x_i^s(t)) - \gamma_i(x_i^m(t))| + |\delta_i^s(t) - \delta_i^m(t)| \\ &\quad \leq |\gamma_i(x_i^s(t)) + \gamma_i(x_i^m(t))| + |\delta_i^s(t) + \delta_i^m(t)| \\ &\quad = |\gamma_i(x_i^{ms}(t))| + |\delta_i^{ms}((t))| \leq \gamma_i + \delta_i, \\ &\quad i = 1,2,3,4. \end{aligned} \tag{16}$$

where $\gamma_i^m > 0, \gamma_i^s > 0, \delta_i^m > 0, \delta_i^s > 0, \gamma_i > 0$, and $\delta_i > 0$ are unknown positive real constants.

4.2. Problems in the controllers and a possible solution

The literature survey [7–18] substantiates that various control strategies synchronize MSS (10–11), but the state error vector oscillates and has large overshoots. Further, in the steady state, the control efforts show oscillations. These fluctuations introduce systemic risks that affect economic growth and destabilize the financial system leading to economic crises. Further, the feedback control strategies [7–16,18] synchronizing two identical TDCS/FDFC systems follow the nonlinear terms cancellation approach. Following such procedures can have significant effects on the economy. For example, removing the nonlinear terms $x_1^s(t)x_2^s(t)$ and/or $x_1^m(t)x_2^m(t)$ through feedback controller, it would likely reduce investment and economic activity.

The synchronization control methodologies [26,27] use signum functions to deal with uncertainties and improve synchronization convergence rates. Signum functions are discontinuous, and using them in feedback controller design can produce abrupt variations with finite frequency and amplitude in the control signals, known as chattering; it creates oscillations in system state variables. The reported literature [28,29] (among others) replaces the signum functions with the continuous hyperbolic tangent functions in feedback control laws to generate smooth control signals and eradicate chattering. However, despite these controller designs, control signal oscillation still exists due to high state-feedback controller gains and the external forces acting on the system.

Objective 4.1: The aim is to construct a state-feedback control algorithm that synthesizes a chatter-free control signal vector $\mathbf{u}(t) \in R^{4\times 1}$, which establishes faster and smooth synchronization errors (12) convergence to zero without oscillations.

This work proposes designing a robust adaptive control law that forces the synchronization error signals (12) to zero with reduced oscillations in the error trajectories and feedback control signals. The controller design methodology does not eliminate the closed-loop's nonlinear terms.

The following section discusses the structure of the proposed controller to address the problem elaborated above. It develops a design procedure based on the Lyapunov stability analysis theory.

5. Solution to problem

This section analyzes the synchronization error (12) converges to zero, and designs the FDFC system parameters update laws.

5.1. Controller design and parameters update laws

Equation (17) designs the structure of an RDASCS, which computes a control effort $\mathbf{u}(t) \in R^{4\times 1}$ that enforces the slave FDFC system (11) to follow the master FDFC system (10) and satisfies the above Objective 4.1.

$$\begin{aligned}\mathbf{u}(t) = &-\mathbf{K}\mathrm{e}^{-\rho|\mathbf{e}(t)|}\mathbf{e}(t) - \boldsymbol{\Psi}(t)\tanh\mathbf{e}(t) - \varphi(\hat{\boldsymbol{\gamma}}(t) \\ &+ \hat{\boldsymbol{\delta}}(t)) \circ \tanh(\mu\mathbf{e}(t)), \end{aligned} \tag{17}$$

where $\boldsymbol{\Psi}(t) = [\psi_{ij}(t), \psi_{ij}(t) = 0 \text{ for } i \neq j]_{4\times 4}$ and $\psi_{ij}(t) = [\psi_{ii}(I_{ii} - \varrho\mathrm{e}^{-\rho|e_i(t)|})]_{4\times 4}$.

Theorem 5.1: *If the feedback controller* (17) *is added to the slave FDFC system in* (11) *and the adaptive laws in* (18) *estimate the unknown parameters* $\hat{\boldsymbol{\gamma}}(t)$ *and* $\hat{\boldsymbol{\delta}}(t)$, *then the dynamical error system* (12) *converges to the vicinity of zero.*

$$\begin{aligned}&\left\{\dot{\hat{\boldsymbol{\gamma}}}(t) = \dot{\hat{\boldsymbol{\delta}}}(t) = -\frac{1}{\sigma}|\boldsymbol{e}(t)|, \hat{\boldsymbol{\gamma}}(0) = \hat{\boldsymbol{\gamma}}_0\right., \\ &\quad \textit{and } \hat{\boldsymbol{\delta}}(0) = \hat{\boldsymbol{\delta}}_0, \end{aligned} \tag{18}$$

where $\hat{\boldsymbol{\gamma}}_0$ and $\hat{\boldsymbol{\delta}}_0$ are the initial values of $\hat{\boldsymbol{\gamma}}(0)$ and $\hat{\boldsymbol{\delta}}(0)$, respectively.

5.2. Robust stability analysis of the closed-loop

Let us construct the Lyapunov candidate function as follows:

$$V(t) = \frac{1}{2}\mathbf{e}^T(t)\mathbf{e}(t) + \frac{\sigma}{2}(\tilde{\boldsymbol{\gamma}}^T(t)\boldsymbol{\gamma} + \tilde{\boldsymbol{\delta}}^T(t)\boldsymbol{\delta}) \geq 0, \quad (19)$$

provided $||\hat{\boldsymbol{\gamma}}(t)|| \leq \boldsymbol{\gamma}$ and $||\hat{\boldsymbol{\delta}}(t)|| \leq \boldsymbol{\delta}$.

Remark 5.1: $\tilde{\boldsymbol{\gamma}}(t) = \boldsymbol{\gamma} + \hat{\boldsymbol{\gamma}}(t), \tilde{\boldsymbol{\delta}}^T(t) = \boldsymbol{\delta} + \hat{\boldsymbol{\delta}}(t), \tilde{\boldsymbol{\gamma}}^T(t)\boldsymbol{\gamma} \geq 0$ and $\hat{\boldsymbol{\delta}}^T(t)\boldsymbol{\delta} \geq 0$ when $||\hat{\boldsymbol{\gamma}}(t)|| \leq \boldsymbol{\gamma}$ and $||\hat{\boldsymbol{\delta}}(t)|| \leq \boldsymbol{\delta}$, it requires that $\lim_{t\to\infty} \hat{\boldsymbol{\gamma}}(t) = -\boldsymbol{\gamma}$ and $\lim_{t\to\infty} \hat{\boldsymbol{\delta}}(t) = -\boldsymbol{\delta}$ without fluctuations. Therefore, inequality (19) holds.

Remark 5.2: Parameters adaptation laws (18) ensure that $\hat{\boldsymbol{\gamma}}(t) \leq 0$ and $\hat{\boldsymbol{\delta}}(t) \leq 0$ for $\hat{\boldsymbol{\gamma}}(0) = \hat{\boldsymbol{\gamma}}_0$ and $\hat{\boldsymbol{\delta}}(0) = \hat{\boldsymbol{\delta}}_0$.

Remark 5.3: Figure 7(g and h) in the simulation section (6) verify Remarks 5.1 and 5.2, respectively.

Now,

$$\dot{V}(t) = \mathbf{e}^T(t)\dot{\mathbf{e}}(t) + \sigma\left(\dot{\hat{\boldsymbol{\gamma}}}^T(t)\boldsymbol{\gamma} + \dot{\hat{\boldsymbol{\delta}}}^T(t)\boldsymbol{\delta}\right). \quad (20)$$

Using Equations (12) and (17) into (20) imply:

$$\begin{aligned}
\dot{V}(t) &= e_1(t)(-a_1e_1(t) + e_3(t) + e_4(t) \\
&\quad + (x_2^s(t)e_1(t) + x_1^m(t)e_2(t))) \\
&\quad + e_2(t)(-a_2e_2(t) - e_1(t) \\
&\quad \times (x_1^m(t) + x_1^s(t))) + e_3(t)(-e_1(t) - a_3e_3(t)) \\
&\quad + e_4(t)(-a_4e_4(t) - a_5(x_2^s(t)e_1(t) \\
&\quad + x_1^m(t)e_2(t))) - \mathbf{e}^T(t)\mathbf{K}\mathrm{e}^{-\rho|\mathbf{e}(t)|}\mathbf{e}(t) \\
&\quad - \mathbf{e}^T(t)\boldsymbol{\Psi}(t)\tanh\mathbf{e}(t) \\
&\quad + \varphi\mathbf{e}^T(t)((\hat{\boldsymbol{\gamma}}(t) + \hat{\boldsymbol{\delta}}(t)) \circ \tanh\mathbf{e}(\mu t)) \\
&\quad + \mathbf{e}^T(t)(\boldsymbol{\gamma}^{ms}(\mathbf{x}^{ms}(t)) + \boldsymbol{\delta}^{ms}(t)) \\
&\quad + \sigma\left(\dot{\hat{\boldsymbol{\gamma}}}^T(t)\boldsymbol{\gamma} + \dot{\hat{\boldsymbol{\delta}}}^T(t)\boldsymbol{\delta}\right) \\
&= -a_1e_1^2(t) + e_1(t)e_4(t) + e_1(t)e_3(t) \\
&\quad + x_2^s(t)e_1^2(t) + e_1(t)e_2(t)x_1^m(t) \\
&\quad - a_2e_2^2(t) - e_1(t)e_2(t)x_1^m(t) \\
&\quad - e_1(t)e_2(t)x_1^s(t) - e_1(t)e_3(t) \\
&\quad - a_3e_3^2(t) - a_4e_4^2(t) - a_5(x_2^s(t)e_1(t)e_4(t) \\
&\quad + x_1^m(t)e_2(t)e_4(t)) \\
&\quad - \mathbf{e}^T(t)\mathbf{K}\mathrm{e}^{-\rho|\mathbf{e}(t)|}\mathbf{e}(t) \\
&\quad - \mathbf{e}^T(t)\boldsymbol{\Psi}(t)\tanh\mathbf{e}(t) \\
&\quad + \mathbf{e}^T(t)(\boldsymbol{\gamma}^{ms}(\mathbf{x}^{ms}(t)) + \boldsymbol{\delta}^{ms}(t)) \\
&\quad + \varphi\mathbf{e}^T(t)((\hat{\boldsymbol{\gamma}}(t) + \hat{\boldsymbol{\delta}}(t)) \circ \tanh\mathbf{e}(\mu t)) \\
&\quad + \sigma\left(\dot{\hat{\boldsymbol{\gamma}}}^T(t)\boldsymbol{\gamma} + \dot{\hat{\boldsymbol{\delta}}}^T(t)\boldsymbol{\delta}\right) \\
&\leq -(a_1 - |x_2^s(t)|)e_1^2(t) - a_2e_2^2(t) \\
&\quad - a_3e_3^2(t) - a_4e_4^2(t) \\
&\quad - a_5(x_2^s(t)e_1(t)e_4(t) + x_1^m(t)e_2(t)e_4(t)) \\
&\quad - x_1^s(t)e_1(t)e_2(t) \\
&\quad - x_1^s(t)e_1(t)e_2(t) - \sum_1^4(k_{ii}\mathrm{e}^{-\rho|e_i(t)|}e_i(t) \\
&\quad + \Psi_{ii}(t)\tanh e_i(t)) \\
&\quad - \mathbf{e}^T(t)\mathbf{K}\mathrm{e}^{-\rho|\mathbf{e}(t)|}\mathbf{e}(t) \\
&\quad - \mathbf{e}^T(t)\boldsymbol{\Psi}(t)\tanh\mathbf{e}(t) \\
&\quad + \mathbf{e}^T(t)(\boldsymbol{\gamma}^{ms}(\mathbf{x}^{ms}(t)) + \boldsymbol{\delta}^{ms}(t)) \\
&\quad + \varphi\mathbf{e}^T(t)((\hat{\boldsymbol{\gamma}}(t) + \hat{\boldsymbol{\delta}}(t)) \circ \tanh\mathbf{e}(\mu t)) \\
&\quad + \sigma\left(\dot{\hat{\boldsymbol{\gamma}}}^T(t)\boldsymbol{\gamma} + \dot{\hat{\boldsymbol{\delta}}}^T(t)\boldsymbol{\delta}\right) \\
&= -\mathbf{e}^T(t)\mathbf{A}(t)\mathbf{e}(t) + \mathbf{e}^T(t)\mathbf{B}(t)\mathbf{e}(t) \\
&\quad - \mathbf{e}^T(t)\mathbf{K}\mathrm{e}^{-\rho|\mathbf{e}(t)|}\mathbf{e}(t) - \mathbf{e}^T(t)\boldsymbol{\Psi}(t)\tanh\mathbf{e}(t) \\
&\quad + \mathbf{e}^T(t)(\boldsymbol{\gamma}^{ms}(\mathbf{x}^{ms}(t)) + \boldsymbol{\delta}^{ms}(t)) \\
&\quad + \varphi\mathbf{e}^T(t)((\hat{\boldsymbol{\gamma}}(t) + \hat{\boldsymbol{\delta}}(t)) \circ \tanh\mathbf{e}(\mu t)) \\
&\quad + \sigma\left(\dot{\hat{\boldsymbol{\gamma}}}^T(t)\boldsymbol{\gamma} + \dot{\hat{\boldsymbol{\delta}}}^T(t)\boldsymbol{\delta}\right) \\
&= -\mathbf{e}^T(t)\mathbf{Q}(t)\mathbf{e}(t) - \mathbf{e}^T(t)\boldsymbol{\Psi}(t)\tanh\mathbf{e}(t) \\
&\quad + \varphi\mathbf{e}^T(t)(\hat{\boldsymbol{\gamma}}(t) \circ \tanh\mathbf{e}(\mu t)) \\
&\quad + \mathbf{e}^T(t)\boldsymbol{\gamma}^{ms}(\mathbf{x}^{ms}(t)) + \sigma\dot{\hat{\boldsymbol{\gamma}}}^T(t)\boldsymbol{\gamma} \\
&\quad + \varphi\mathbf{e}^T(t)(\hat{\boldsymbol{\delta}}(t) \circ \tanh\mathbf{e}(\mu t)) \\
&\quad + \mathbf{e}^T(t)\boldsymbol{\delta}^{ms}(t) + \sigma\dot{\hat{\boldsymbol{\delta}}}^T(t)\boldsymbol{\delta} \\
&= \dot{V}_{\mathbf{Q}}(t) + \dot{V}_{\boldsymbol{\Psi}}(t) + \dot{V}_{\boldsymbol{\gamma}}(t) + \dot{V}_{\boldsymbol{\delta}}(t), \quad (21)
\end{aligned}$$

where

$$\mathbf{Q}(t) = \mathbf{A}(t) + \mathbf{K}\mathrm{e}^{-\rho|\mathbf{e}(t)|} - \mathbf{B}(t), \quad (22)$$

$$\mathbf{A}(t) = \begin{bmatrix} a_1 - |x_2^s(t)| & 0 & 0 & 0 \\ 0 & a_2 & 0 & 0 \\ 0 & 0 & a_3 & 0 \\ 0 & 0 & 0 & a_4 \end{bmatrix}, \quad (23)$$

$$\begin{aligned}
&e_1(t)e_4(t) - a_5x_2^s(t)e_1(t)e_4(t) - a_5x_1^m(t)e_2(t)e_4(t) \\
&\quad = \mathbf{e}^T(t)\mathbf{B}\mathbf{e}(t), \quad (24)
\end{aligned}$$

$$\mathbf{B}(t) = \begin{bmatrix} 0 & 0 & 0 & 1 - a_5x_2^s(t) \\ 0 & 0 & 0 & -a_5x_1^m(t) \\ 0 & 0 & 0 & 0 \\ 0 & 0 & 0 & 0 \end{bmatrix}, \quad (25)$$

and

$$\begin{cases} \dot{V}_{\mathbf{Q}}(t) = -\mathbf{e}^T(t)\mathbf{Q}(t)\mathbf{e}(t), \\ \dot{V}_{\boldsymbol{\Psi}}(t) = -\mathbf{e}^T(t)\boldsymbol{\Psi}(t)\tanh\mathbf{e}(t), \\ \dot{V}_{\boldsymbol{\gamma}}(t) = \varphi\mathbf{e}^T(t)(\hat{\boldsymbol{\gamma}}(t)\circ\tanh\mathbf{e}(\mu t)) \\ +\mathbf{e}^T(t)\boldsymbol{\gamma}^{ms}(\mathbf{x}^{ms}(t)) + \sigma\dot{\hat{\boldsymbol{\gamma}}}^T(t)\boldsymbol{\gamma}, \\ \dot{V}_{\boldsymbol{\delta}}(t) = \varphi\mathbf{e}^T(t)(\hat{\boldsymbol{\delta}}(t)\circ\tanh\mathbf{e}(\mu t)) + \mathbf{e}^T(t)\boldsymbol{\delta}^{ms}(t) \\ +\sigma\dot{\hat{\boldsymbol{\delta}}}^T(t)\boldsymbol{\delta}. \end{cases} \tag{26}$$

5.3. Stability analysis of $\dot{V}_{\mathbf{Q}}(t)$, $\dot{V}_{\boldsymbol{\Psi}}(t)$, $\dot{V}_{\boldsymbol{\gamma}}(t)$, and $\dot{V}_{\boldsymbol{\delta}}(t)$

5.3.1. Analysis of $\dot{V}_{\mathbf{Q}}(t)$ and $\dot{V}_{\boldsymbol{\Psi}}(t)$

Let us choose $k_{ii} > 0$ and $\psi_{ii} > 0$, which assures that $\mathbf{Q}(t) > 0$ and $\mathbf{e}^T(t)\boldsymbol{\Psi}(t)\tanh\mathbf{e}(t) \geq 0$; consequently $\dot{V}_{\mathbf{Q}}(t) \leq 0$ and $\dot{V}_{\boldsymbol{\Psi}}(t) \leq 0$.

5.3.2. Analysis of $\dot{V}_{\boldsymbol{\gamma}}(t)$ and $\dot{V}_{\boldsymbol{\delta}}(t)$

To show that $\dot{V}_{\boldsymbol{\gamma}}(t) \leq 0$ and $\dot{V}_{\boldsymbol{\delta}}(t) \leq 0$, consider,

$$\begin{aligned} \dot{V}_{\boldsymbol{\gamma}}(t) &= \varphi\mathbf{e}^T(t)(\hat{\boldsymbol{\gamma}}(t)\circ\tanh\mathbf{e}(\mu t)) \\ &\quad + \mathbf{e}^T(t)\boldsymbol{\gamma}^{ms}(\mathbf{x}^{ms}(t)) + \sigma\dot{\hat{\boldsymbol{\gamma}}}^T(t)\boldsymbol{\gamma} \\ &\leq \varphi\mathbf{e}^T(t)(\hat{\boldsymbol{\gamma}}(t)\circ\tanh\mathbf{e}(\mu t)) \\ &\quad + |\mathbf{e}^T(t)\boldsymbol{\gamma}^{ms}(\mathbf{x}^{ms}(t))| + \sigma\dot{\hat{\boldsymbol{\gamma}}}^T(t)\boldsymbol{\gamma} \\ &\leq \varphi\mathbf{e}^T(t)(\hat{\boldsymbol{\gamma}}(t)\circ\tanh\mathbf{e}(\mu t)) \\ &\quad + \boldsymbol{\gamma}^T|\mathbf{e}(t)| + \sigma\dot{\hat{\boldsymbol{\gamma}}}^T(t)\boldsymbol{\gamma}. \end{aligned} \tag{27}$$

Using update laws (18) in Equation (27) gives:

$$\begin{aligned} \dot{V}_{\boldsymbol{\gamma}}(t) &\leq \varphi\mathbf{e}^T(t)(\hat{\boldsymbol{\gamma}}(t)\circ\tanh\mathbf{e}(\mu t)) \\ &\quad + \boldsymbol{\gamma}^T|\mathbf{e}(t)| - \boldsymbol{\gamma}^T|\mathbf{e}(t)| \\ &\leq \varphi\mathbf{e}^T(t)(\hat{\boldsymbol{\gamma}}(t)\circ\tanh\mathbf{e}(\mu t)) \leq 0, \end{aligned} \tag{28}$$

because $\hat{\boldsymbol{\gamma}}(t) \leq 0$.

Similarly, it can also be shown that:

$$\dot{V}_{\boldsymbol{\delta}}(t) = \varphi\mathbf{e}^T(t)(\hat{\boldsymbol{\delta}}(t)\circ\tanh\mathbf{e}(\mu t)) \leq 0 \tag{29}$$

Therefore,

$$\dot{V}(t) = \dot{V}_{\mathbf{Q}}(t) + \dot{V}_{\boldsymbol{\Psi}}(t) + \dot{V}_{\boldsymbol{\gamma}}(t) + \dot{V}_{\boldsymbol{\delta}}(t) \leq 0. \tag{30}$$

The inequality (30) determines that the error vector trajectories converge in the origin's vicinity. The unknown controller parameter estimations are associated with the exogenous disturbances and uncertainties and approach some constant values. Hence, the closed-loop (12) global asymptotic stability is proved [17]; it establishes that $\lim_{t\to\infty}\mathbf{e}(t) = 0$. □

Remark 5.4: Figure 8(a–d) depicts that the synchronization speed increases with large values of k_{ii} and ψ_{ii}.

6. Numerical simulations and comparative study

Table 3 assumes the initial conditions, FDFC system parameters, controller parameters, exogenous disturbances, and model uncertainties in numerical simulations.

The state-variable trajectories $x_i(t)$, $i = 1, 2, 3, 4$ in Figure 6(a–d) and error vector trajectories in Figure 6(e) demonstrate that the MSS (10–11) do not synchronize without any control effort.

Example 6.1: In this example, Figure 7(a–h) simulation results are performed under the control effort computed using the proposed RDASCS (17). Figure 7(a–d) demonstrates that the corresponding state variables $x_i^m(t)$ and $x_i^s(t)$, $i = 1, 2, 3, 4$ trajectories of the MSS (10–11) show similar behaviour after a short transient time. Figure 7(e) illustrates that the error trajectories converge to the origin smoothly in less than 0.05 s with significantly reduced fluctuations. Figure 7(f) shows the synchronization error vector convergence in the range $[-0.002, 0.002]$. In this figure, blue trajectories are $y_1(t) = 0.00053e^{-0.0071\,t} + 0.00147e^{-0.18\,t}$ and $y_2(t) = -y_1(t)$ represent the convergence behaviour of the $\mathbf{e}(t)$. These trajectories are obtained using four points from the maximum oscillations of $\mathbf{e}(t)$ simulation data at $t = 0$, 20, 40, and 80 seconds. It is obvious that $\lim_{t\to\infty} y_1(t) = 0$ validating $\lim_{t\to\infty}\mathbf{e}(t) = 0$, which is consistent with the theoretical findings in Subsection 5.3.

Table 3. Initial conditions, FDFC system parameters, controller parameters, exogenous disturbances, and model uncertainties.

Initial conditions	Parameters of the FDFC system	Parameters of the controller	Model uncertainties	Exogenous disturbances
$x_1^m(0) = -0.5$,	$a_1 = 0.9$,	$k_{ii} = 1$,	$\gamma_1^m(x_1^m(t)) = 0.3\sin 4x_1^m(t)$,	$\delta_1^m(t) = -0.4\cos 5t$,
$x_2^m(0) = 1$,	$a_2 = 0.2$,	$\psi_{ii} = 1$,	$\gamma_2^m(x_2^m(t)) = -0.2\cos 2x_2^m(t)$,	$\delta_2^m(t) = -0.2\sin 4t$,
$x_3^m(0) = 1$,	$a_3 = 1.5$,	$\sigma = 60$,	$\gamma_3^m(x_3^m(t)) = 0.1\sin 4x_3^m(t)$,	$\delta_3^m(t) = 0.1\cos t$,
$x_4^m(0) = 2$,	$a_4 = 0.2$,	$\rho = 0.01$,	$\gamma_4^m(x_4^m(t)) = 0.15\sin x_3^m(t)$,	$\delta_4^m(t) = -0.1\cos 3t$,
$x_1^s(0) = -1$,	$a_5 = 0.17$	$\mu = 30$,	$\gamma_1^s(x_1^s(t)) = 0.15\sin 4x_1^s(t)$,	$\delta_1^s(t) = 0.2\cos 5t$,
$x_2^s(0) = 2.5$,		$\varrho = 0.5$,	$\gamma_2^s(x_2^s(t)) = 0.1\sin 2x_2^s(t)$,	$\delta_2^s(t) = 0.2\sin 5t$,
$x_3^s(0) = 1.7$,		$\varphi = 10$	$\gamma_3^s(x_3^s(t)) = 0.15\cos x_3^s(t)$,	$\delta_3^s(t) = 0.1\sin 3t$,
$x_4^s(0) = 1$,			$\gamma_4^s(x_4^s(t)) = -0.1\cos 2x_3^s(t)$	$\delta_4^s(t) = 0.15\sin 5t$
$\hat{\gamma}_{i0} = 0$,				
$\hat{\delta}_{i0} = 0$				

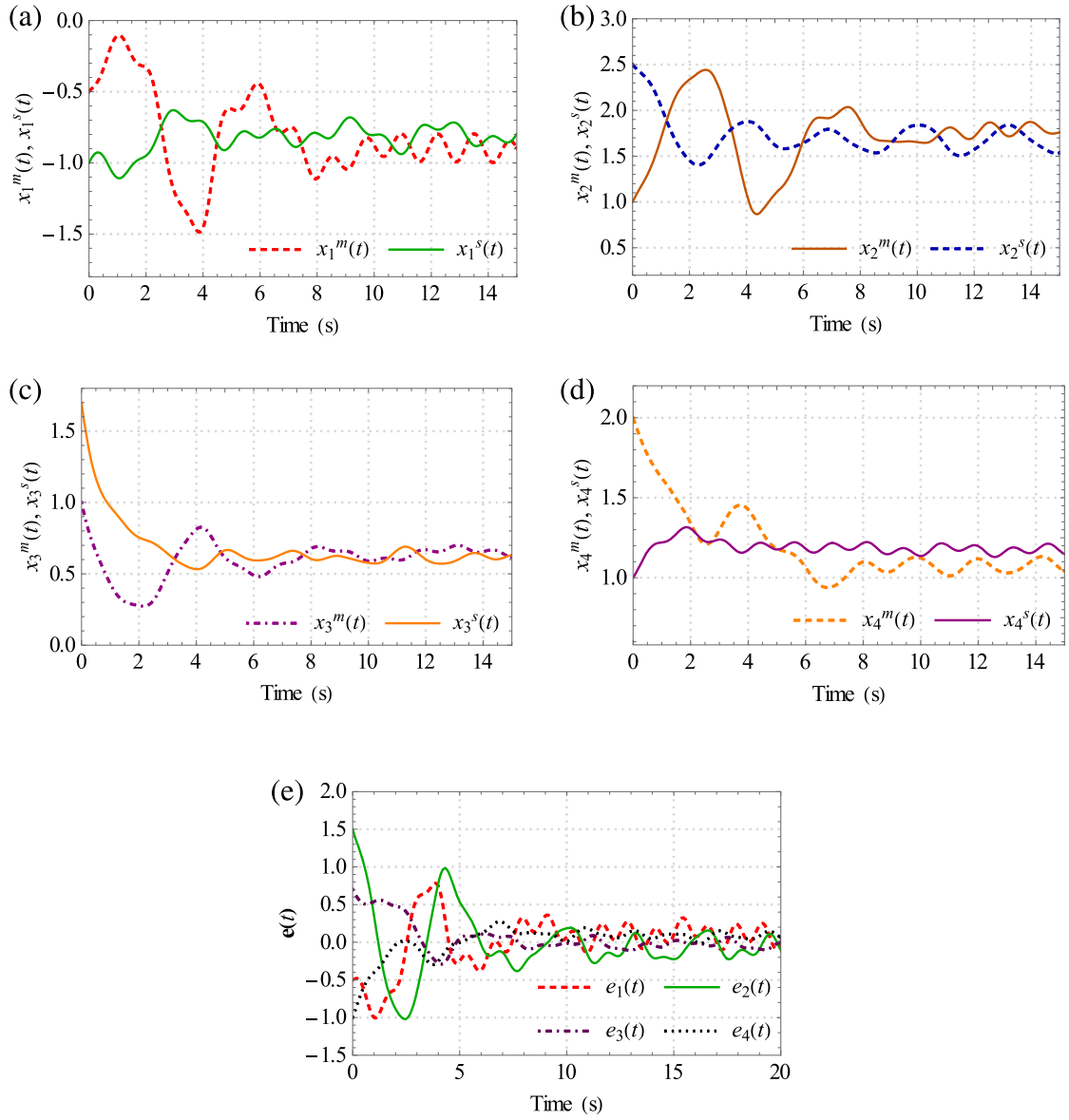

Figure 6. (a) The unsynchronized behaviour of the state variables $x_1^m(t)$ and $x_1^s(t)$ without control inputs; (b) The unsynchronized behaviour of the state variables $x_2^m(t)$ and $x_2^s(t)$ without control inputs; (c) The unsynchronized behaviour of the state variables $x_3^m(t)$ and $x_3^s(t)$ without control inputs; (d) The unsynchronized behaviour of the state variables $x_4^m(t)$ and $x_4^s(t)$ without control inputs; (e) The synchronization errors transient behaviour without a control effort.

Figure 7(g–h) depicts the convergence of the estimated parameters $\hat{\boldsymbol{\gamma}}(t)$ and $\hat{\boldsymbol{\delta}}(t)$ using the parameter update laws (18).

Example 6.2: This example discusses the effects of feedback controller gains on the error vector convergence behaviour.

The convergence behaviour of the errors vector for different controller gains k_{ii} and ψ_{ii} are shown in Figure 8(a–d). These figures demonstrate that the convergence speed of the errors vector increases, and the error oscillation's amplitude decreases when the values of k_{ii} and ψ_{ii} are considered large. Table 4 summarizes the data for the simulation results shown in Figure 8(a–d).

6.1. Robust analysis of the closed-loop

Example 6.3: This example studies the effects of exogenous disturbances and 10% smooth FDFC system parameters variations on the performance of the closed-loop.

Scenario 1: When no exogenous disturbances act on the MSS (10–11).
Scenario 2: Effects of exogenous disturbances

$$\delta_i^m(t) = \frac{0.5}{t^2+3}, \quad \delta_i^s(t) = 0.7\cos\left(0.2\frac{\pi}{3}t\right) \quad (31)$$

Scenario 3: Effects of 10% smooth FDFC system parameters variations

$$a_1 = 0.9 + 0.09e^{-0.01t}, a_2 = 0.2 + 0.02e^{-0.01t},$$
$$a_3 = 1.5 + 0.15e^{-0.01t},$$

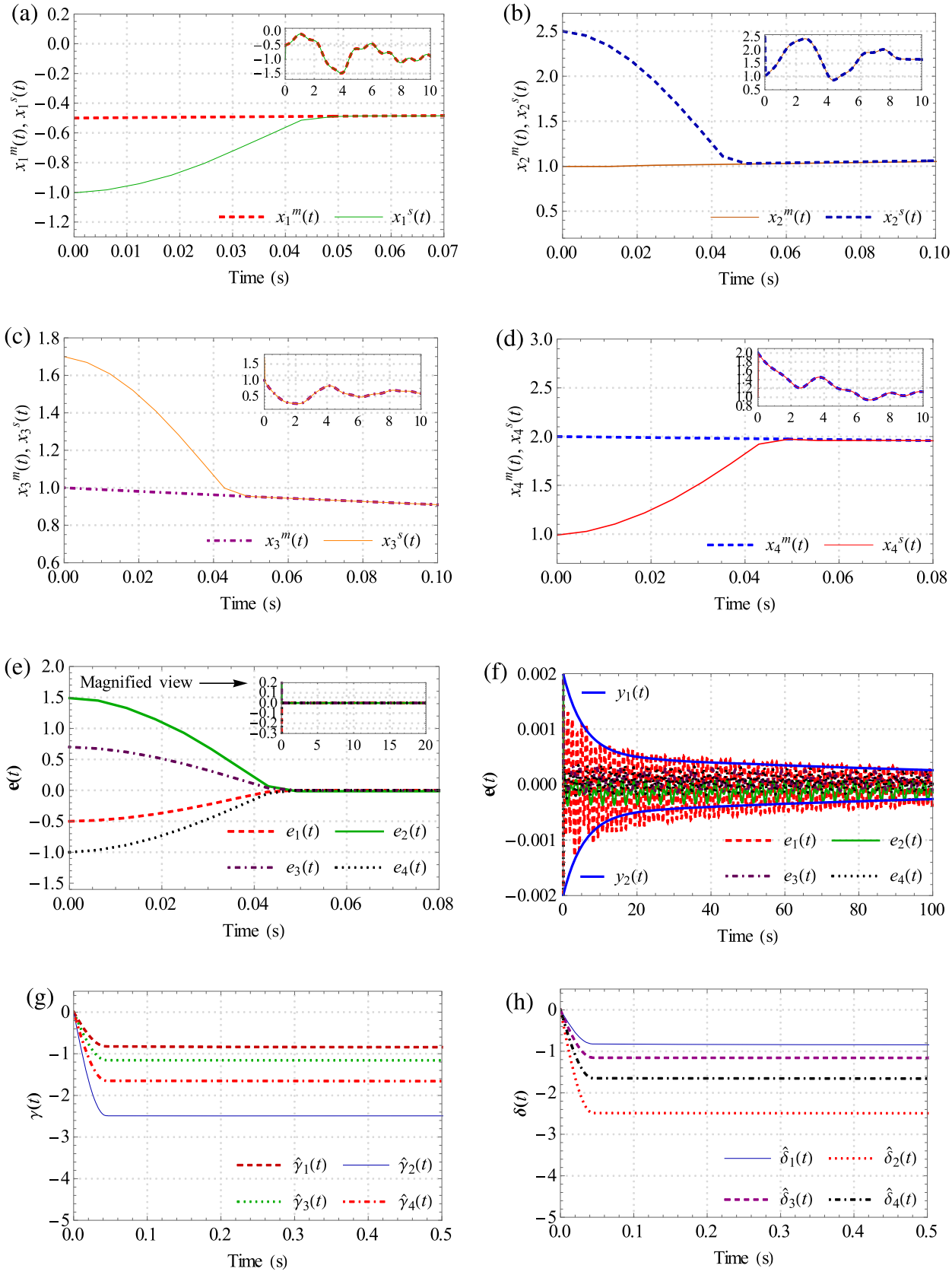

Figure 7. (a) The MSS state variables $x_1^m(t)$ and $x_1^s(t)$ behaviour with control input (17); (b) The MSS state variables $x_2^m(t)$ and $x_2^s(t)$ behaviour with control input (17); (c) The MSS state variables $x_3^m(t)$ and $x_3^s(t)$ behaviour with control input (17); (d) The MSS state variables $x_4^m(t)$ and $x_4^s(t)$ behaviour with control input (17); (e) Convergence of the synchronization error signals; (f) Convergence of the synchronization error vector in the range $[-0.002, 0.002]$; (g) Convergence behaviour of the estimated parameters $\hat{\gamma}_i(t), i = 1, 2, 3, 4$; (h) Convergence behaviour of the estimated parameters $\hat{\delta}_i(t), i = 1, 2, 3, 4$.

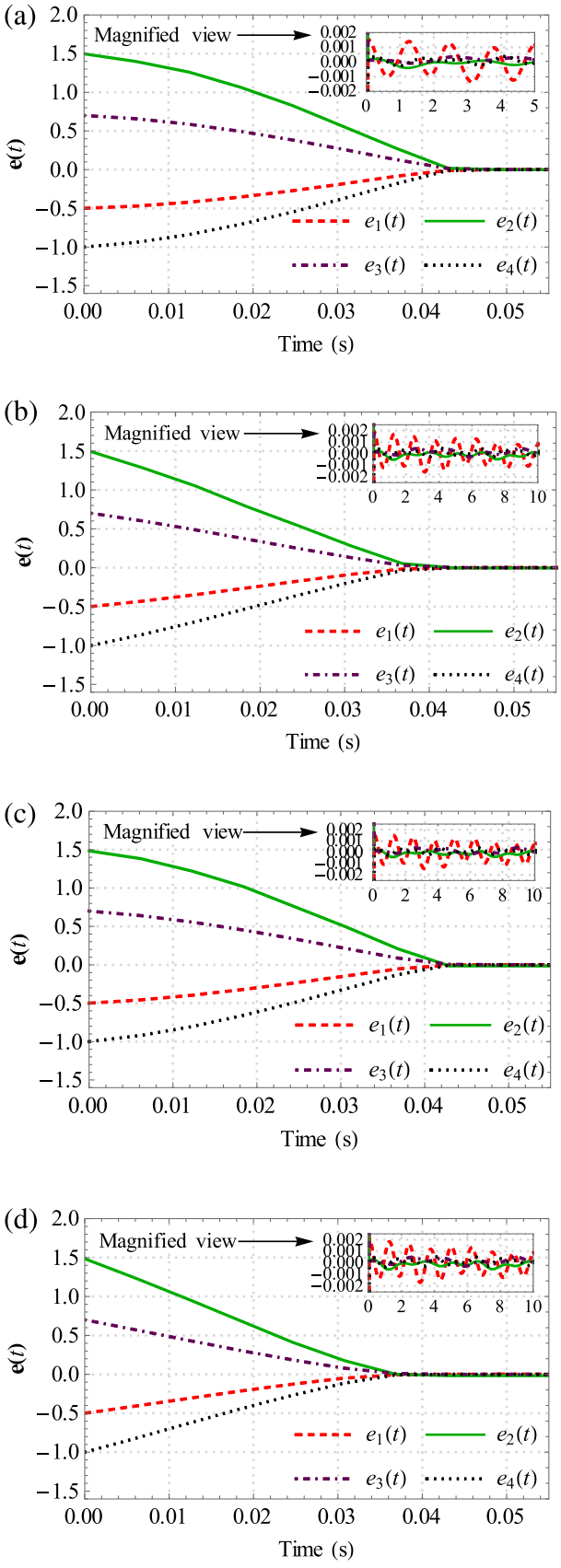

Figure 8. (a) Errors vector behaviour with a control effort (17) when $k_{ii} = 5$, $\psi_{ii} = 1$; (b) Errors vector behaviour with a control effort (17) when $k_{ii} = 20$, $\psi_{ii} = 1$; (c) Errors vector behaviour with a control effort (17) when $k_{ii} = 1$, $\psi_{ii} = 20$; (d) Errors vector behaviour with a control effort (17) when $k_{ii} = 20$, $\psi_{ii} = 20$.

Table 4. Comparison of the computer simulation results.

S. No	Feedback gains	Convergence time	Range of error signals oscillations
1	$k_{ii} = 5, \psi_{ii} = 1$	0.044*s*	[−0.0015, 0.0015]
2	$k_{ii} = 20, \psi_{ii} = 1$	0.042*s*	[−0.001, 0.001]
3	$k_{ii} = 1, \psi_{ii} = 20$	0.044*s*	[−0.0008, 0.0008]
4	$k_{ii} = 20, \psi_{ii} = 20$	0.038*s*	[−0.0005, 0.0005]

$$a_4 = 0.17 + 0.017e^{-0.01t}, a_5 = 0.2 + 0.02e^{-0.01t} \tag{32}$$

Figure 9(a–c) illustrates the error trajectories convergence behaviour to zero by the proposed method (17) for Scenarios 1–3, alternatively. These figures demonstrate that the proposed controller is robust to exogenous disturbances and smooth FDFC system parameter variations, and the convergence time is less than 0.05 s.

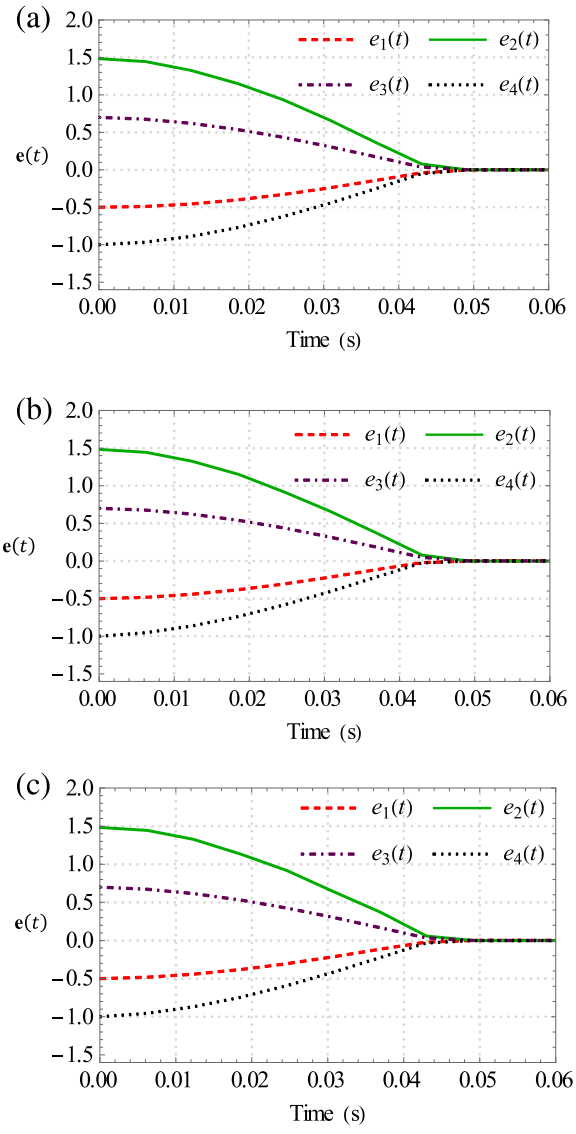

Figure 9. (a) Errors vector behaviour for Example 3, Scenario 1; (b) Errors vector behaviour for Example 3, Scenario 2; (c) Errors vector behaviour for Example 3, Scenario 3.

The robust performance of two identical hyperchaotic finance systems synchronization is helpful for predictive analytics and improved security, which can benefit financial forecasting, risk management, and protection against cyber-attacks. By analyzing the synchronized data, it is possible to identify patterns and trends that can be used to make more informed financial decisions and enhance the overall system's security.

6.2. Comparative analysis

Example 6.4 presents the computer simulation results of the proposed method (17) and compares it with the feedback controllers proposed in recent published research articles [13,22], addressing the synchronization of similar chaotic dynamic systems. The comparative study is based on synchronization errors and control effort behaviour analysis in this context. The significance of these variables is as follows.

Errors: Fast synchronization of two identical hyperchaotic finance systems with reduced fluctuations of the error signals can improve the accuracy of the financial forecasts, which often rely on precise timing. Further, it reduces the risk of errors or discrepancies between the two systems and can help to prevent losses and other financial problems.
Control efforts: The smooth control effort is inherently robust to model uncertainties and disturbances in the system; the synchronization process is less likely to be affected by external factors, such as disturbances or variations in the system parameters. Further, it reduces the system's overall energy consumption and makes synchronization more efficient.

Therefore, to make the comparison systematic, the analysis describes these two variables in detail and summarizes essential performance indicators in Tables 5–7. The following describes these indicators.

Example 6.4: The state-feedback control input vector $\mathbf{u}(t) \in R^{4\times 1}$ synthesized by the sliding mode control (SMC) strategy (33) and adaptive controller (34) reported in [22] and [13], respectively. For the benchmark, initial conditions, model uncertainties, exogenous disturbances, FDFC system (2) parameters, and controller parameters are selected as given in Table 3.

Table 6. Comparison of *IAE*, *ITAE*, and *ISE*.

Index	Error	RDASCS (17)	SMC (33)	Adaptive controller (34)
$IAE = \int_0^{Ts} \lvert e(t)\rvert dt$	$e_1(t)$	0.0339	1.1422	1.9635
	$e_2(t)$	0.0466	1.5949	1.0358
	$e_3(t)$	0.0268	0.3764	1.7517
	$e_4(t)$	0.0333	0.7673	1.6374
$ITAE = \int_0^{Ts} \lvert e(t)\rvert tdt$	$e_1(t)$	0.1296	7.2787	12.453
	$e_2(t)$	0.0372	5.4406	0.6373
	$e_3(t)$	0.0509	1.4401	8.0101
	$e_4(t)$	0.0421	2.7848	7.9899
$ISE = \int_0^{Ts} e^T(t)e(t)dt$	$e_1(t)$	0.0054	0.1414	0.4249
	$e_2(t)$	0.0482	0.9227	0.9308
	$e_3(t)$	0.0105	0.0913	0.4706
	$e_4(t)$	0.0212	0.2575	0.5348

(i) Sliding mode control strategy [22]:

$$\mathbf{u}(t) = \begin{bmatrix} \hat{a}_1(t) - k_{11} & 0 & 1 & 1 \\ 0 & \hat{a}_2(t) - k_{22} & 0 & 0 \\ 1 & 0 & \hat{a}_3(t) - k_{33}(t) & 0 \\ 0 & 0 & 0 & \hat{a}_4(t) - k_{44}(t) \end{bmatrix} \mathbf{e}(t) - \begin{bmatrix} -\psi_{11} & 0 & 1 & 1 \\ 0 & -\psi_{22} & 0 & 0 \\ 1 & 0 & -\psi_{33}(t) & 0 \\ 0 & 0 & 0 & -\psi_{44}(t) \end{bmatrix} \operatorname{sgn}(\mathbf{e}(t)) - \begin{bmatrix} x_2^s(t)e_1(t) \\ -e_1(t)(x_1^m(t) + x_1^s(t)) \\ 0 \\ -a_5(x_2^s(t)e_1(t) + x_1^m(t)e_2(t)) \end{bmatrix} \tag{33}$$

According to [22], $k_{ii} > 0$ $(i = 1, 2, 3, 4)$ is the controller parameter, $s_i(t) = \psi_{ii}\operatorname{sgn}(e_i(t)) \in R$, $\mathbf{s}(t) = [s_1(t) \quad s_2(t) \quad s_3(t) \quad s_4(t)]^T \in R^{4\times 1}$ is the switching surface, and $\psi_{ii} > 0$ is the switching surface parameter.

Table 5. Comparison of the computer simulation results.

Controller/Feedback gains	Figure No/ Errors convergence time	Range of the errors oscillations in the steady-state	Figure No/Range of the control signals oscillations
RDASCS (17)/ $k_{ii} = 1$, $\psi_{ii} = 1$ $i = 1, 2, 3, 4$	Figure 7(e)/0.05s	[−0.0015, 0.0015]	Figure 11(a)/[−0.8, 0.8]
SMC technique (33)/ $k_{ii} = 1$, $\psi_{ii} = 0.01$ $i = 1, 2, 3, 4$	Figure 10(a)/ steady state does not establish	[−0.2, 0.15]	Figure 11(b)/[−1.5, 1.5]
Adaptive controller (34)/ $k_{ii} = 1, i = 1, 2, 3, 4,$	Figure 10(b)/ steady state does not establish	Lose synchronization	Diverges

Table 7. Comparison of the rate of dissipation of the energy function.

Control input	Lyapunov function	Lyapunov function gradient
RDASCS (17)	$V(t)$ in (19)	$\dot{V}(t) \leq \dot{V}_{\mathrm{Q}}(t) + \dot{V}_{\Psi}(t)$
SMC technique (33)	$V_1(t) = \frac{1}{2}\sum_{i=1}^{4} \psi_{ii}^2 e_i^2(t)$	$\dot{V}_1(t) = -\sum_{i=1}^{4} \psi_{ii}^2 e_i^2(t) - \sum_{i=1}^{4} \psi_{ii}\lvert e_i(t)\rvert$
Adaptive controller (34)	$V_2(t) = \frac{1}{2}\mathrm{e}^T(t)\mathrm{e}(t) + \frac{1}{2}\sum_{i=1}^{4} \tilde{a}_i^2(t)$, $\tilde{a}_i(t) = \hat{a}_i(t) - a_i, i = 1,2,3,4$	$\dot{V}_2(t) = -\sum_{i=1}^{4} k_{ii} e_i^2(t)$

Performance indicator	:	Description
Error convergence time	:	During this time, the synchronization error converges to zero vicinity, and the system state variables approach the steady state. A faster synchronization error convergence requires a shorter error convergence time.
Error oscillation range	:	It is the range of synchronization error oscillation in the steady state. A smaller error oscillation range improves the financial forecast accuracy.
Control effort oscillation range	:	This range indicates the upper and lower peak limits of the control effort. Shorter control effort range refers to lower energy consumption requirements for synchronization.
Synchronization error energy function	:	It is defined by $\boldsymbol{\eta}(t) = \frac{1}{2}\mathrm{e}^T(t)\mathrm{e}(t)$.
Gradient of the synchronization error energy function	:	Gradient of the energy function is defined as $\dot{\boldsymbol{\eta}}(t) = \mathrm{e}^T(t)\dot{\mathrm{e}}(t)$. When the gradient of an energy function becomes zero quickly can lead to improved closed-loop stability, reduced computation time, and increased synchronization accuracy.
Lyapunov function, $V(t)$	:	It represents the closed-loop system variables' total energy.
Lyapunov function gradient, $\dot{V}(t)$	:	It is the closed-loop system variables' total energy gradient.
The following three performance indices are commonly used in control systems error analysis.		
Integral of absolute error, $IAE = \int_0^{Ts} \lvert\mathrm{e}(t)\rvert dt$	:	The *IAE* is the cumulative absolute synchronization error measure over time. Smaller *IAE* implies better aggregate synchronization behaviour; it does not show instantaneous behaviour.
Integral of the time absolute error, $ITAE = \int_0^{Ts} t\lvert\mathrm{e}(t)\rvert dt$	:	*ITAE* is a modified version of *IAE* that takes into account the synchronization error duration as well. It is integral to the time multiplied by the magnitude of the error over a specified period. Lower *ITAE* means quicker and more accurate synchronization attitude.
Integral of the square error, $ISE = \int_0^{Ts} \mathrm{e}^T(t)\mathrm{e}(t)dt$	:	It is a cumulative square of the synchronization error measure over time, a frequently used control system error analysis performance index. Its quantitative importance is similar to *IAE*, but offers mathematical advantages in the design process.

(ii) The adaptive control technique [13]:

$$\mathbf{u}(t) = \begin{bmatrix} \hat{a}_1(t) - k_{11} & 0 \\ 0 & \hat{a}_2(t) - k_{22} \\ 1 & 0 \\ 0 & 0 \end{bmatrix} \begin{bmatrix} -1 & -1 \\ 0 & 0 \\ \hat{a}_3(t) - k_{33}(t) & 0 \\ 0 & \hat{a}_4(t) - k_{44}(t) \end{bmatrix} \mathbf{e}(t) - \begin{bmatrix} x_2^s(t)e_1(t) \\ -e_1(t)(x_1^m(t) + x_1^s(t)) \\ 0 \\ -a_5(x_2^s(t)e_1(t) + x_1^m(t)e_2(t)) \end{bmatrix} \quad (34)$$

where k_{ii} $(i = 1,2,3,4)$ indicate the correlation coefficient and $\hat{a}_i(t)$ $(i = 1,2,3,4)$ are the adaptive parameters [13].

Figure 7(e) depicts the error vector convergence behaviour accomplished by the proposed RDASCS (16), and Figure 10(a and b) illustrate the error vector behaviour by the controllers (33) and (34), respectively. These figures demonstrate that the proposed RDASCS (17) establishes the synchronization in 0.05 seconds with less active oscillations. Figure 10(a) shows oscillatory

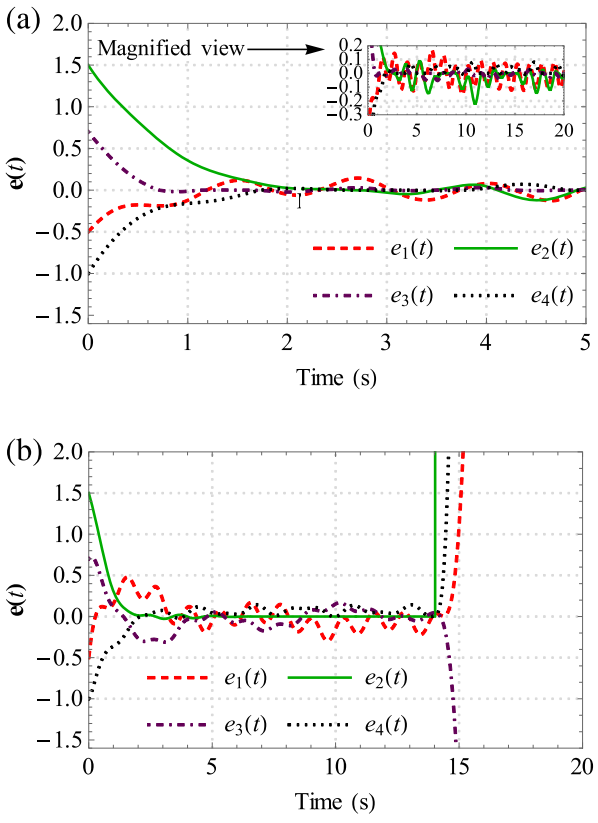

Figure 10. (a) Errors vector behaviour by the SMC strategy (33); (b) Errors vector behaviour by the adaptive control strategy (34).

behaviour, and the error vector does not achieve a steady-state and oscillates in the range $[-0.2, 0.15]$. The error signals from the adaptive controller (34) lose synchronization behaviour after 15 s, as shown in Figure 10(b).

Figure 11(a) illustrates the proposed controller (17) transient behaviour showing oscillations in the range $[-0.8.0.8]$; it takes appropriate action to compel the state errors vector to the origin. The control signals of the SMC strategy (33) exhibit chattering behaviour and oscillate in the range $[-1.5, 1.5]$, i.e. the steady state does not establish. The control input signals of the adaptive controller in (34) remain oscillatory, as illustrated in Figure 11(c), and it diverges after 15 s.

Table 5 provides essential performance indicators regarding errors convergence time, steady-state oscillation range, and control signals amplitude range shown in Figures 7(e), 10(a–b) and 11(a–c).

Table 6 summarizes the standard error performance indices-based comparative simulation studies of synchronization errors [30] for the simulation duration $T_s = 100$ seconds. This simulation analytic data verifies that the proposed RDASCS (17) performs better than the other controllers (33, 34) in all the performance indices.

The synchronization energy error behaviour for the proposed algorithm (17), SMC strategy (33), and the adaptive controller (34) are defined as $\boldsymbol{\eta}(t) = \boldsymbol{\eta}_1(t) = \boldsymbol{\eta}_2(t) = \frac{1}{2}\mathbf{e}^T(t)\mathbf{e}(t)$. Simulation results in Figure 12(a) show that the proposed controller (17) brings the system synchronization error energy to zero steady-state in less than 0.046 s, while $\boldsymbol{\eta}_1(t)$ and $\boldsymbol{\eta}_2(t)$ do not converge. Figure 12(b) illustrates that $\boldsymbol{\eta}_1(t)$ converges in 1.5 s, and $\boldsymbol{\eta}_2(t)$ does not converge; it remains oscillating until the end of the simulation time, two seconds.

Table 7 compares the energy dissipation rate regarding the Lyapunov function gradient.

The inequality (35) is obtained using Table 6.

$$|\dot{V}_2(t)| \leq |\dot{V}_1(t)| \leq |\dot{V}(t)|. \tag{35}$$

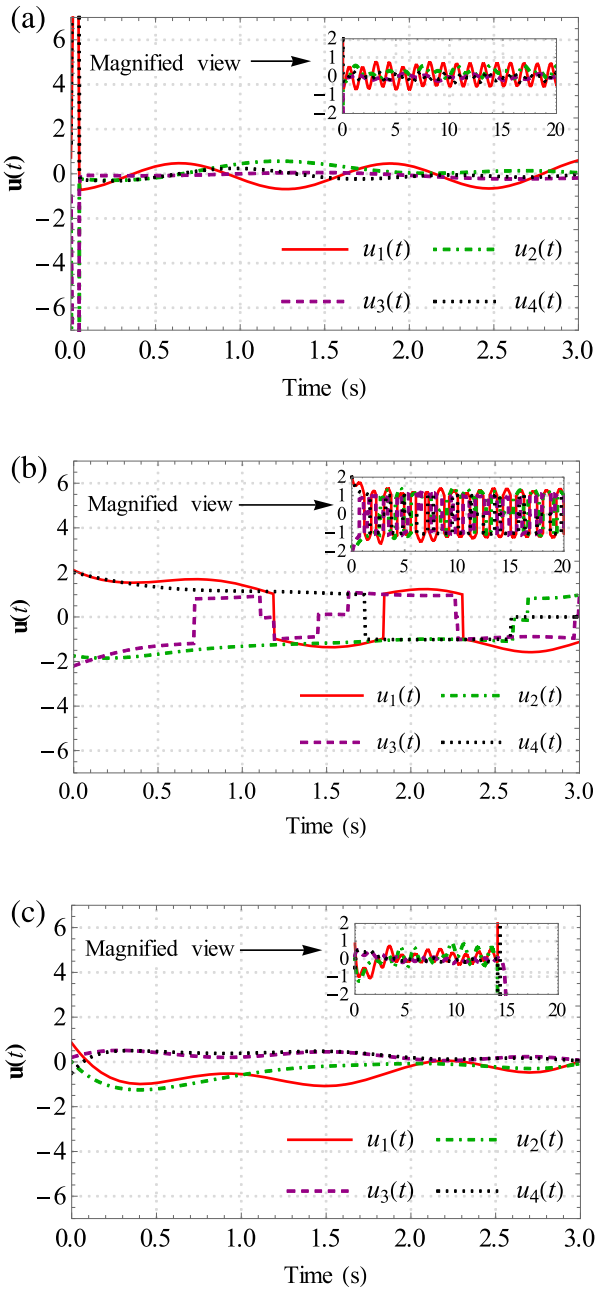

Figure 11. (a) The transient behaviour of the proposed RDASCS signals (17); (b) The transient behaviour of the proposed RDASCS signals (33); (c) The transient behaviour of the adaptive controller signals (34).

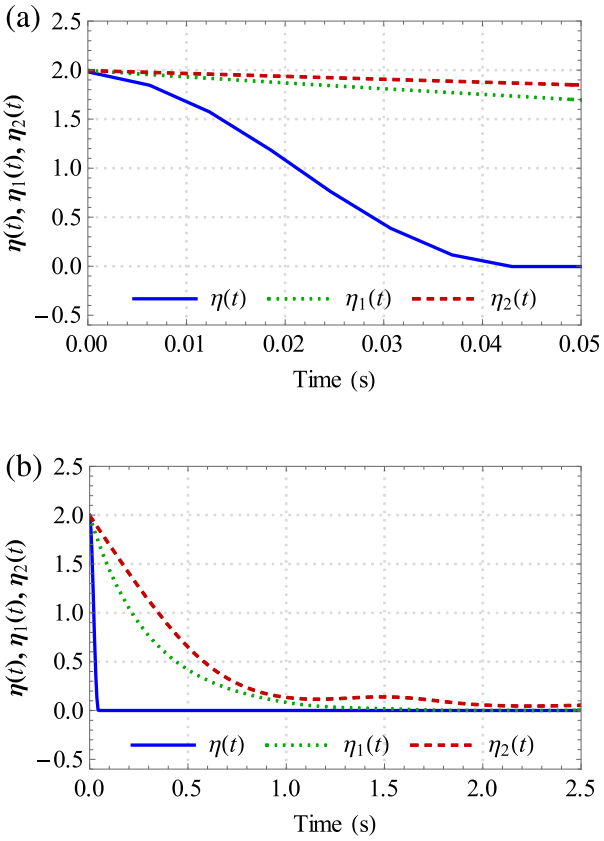

Figure 12. (a) Comparison of $\boldsymbol{\eta}(t)$, $\boldsymbol{\eta}_1(t)$, and $\boldsymbol{\eta}_2(t)$ for 0.05 s; (b) Comparison of $\boldsymbol{\eta}(t)$, $\boldsymbol{\eta}_1(t)$, and $\boldsymbol{\eta}_2(t)$ for 2.5 s.

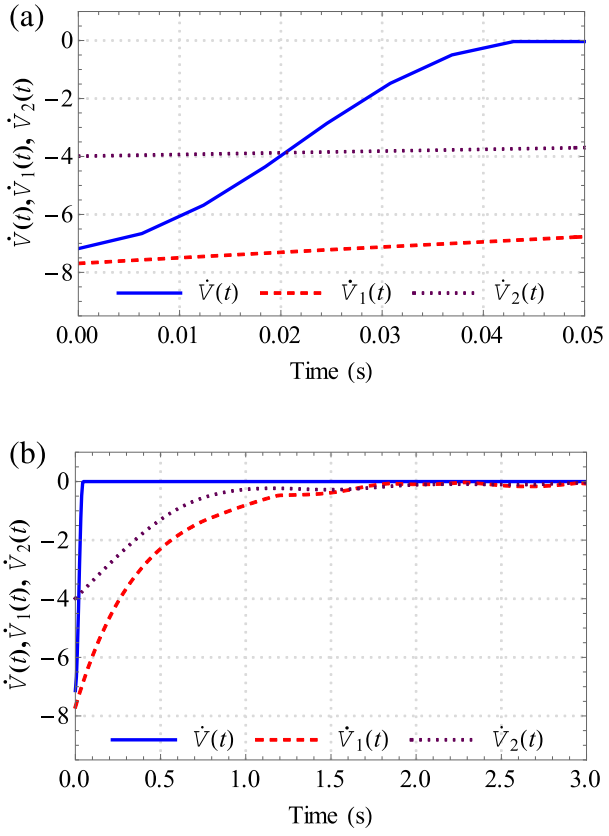

Figure 13. (a) Comparison of $\dot{V}(t)$, $\dot{V}_1(t)$, and $\dot{V}_2(t)$ for 0.05 s; (b) Comparison of $\dot{V}(t)$, $\dot{V}_1(t)$, and $\dot{V}_2(t)$ for 3 s.

Figure 13(a) shows the behaviour of energy dissipation rate functions $\dot{V}(t)$ and $\dot{V}_i(t)$, $i = 1, 2$ accomplished by controllers (17), (33), and (34), alternatively for 0.05 s and Figure 13(b) for 3 s.

The time gradient of a constant synchronization error energy function is zero. $\dot{V}(t)$ stays at zero after 0.044 s, indicating the closed-loop remains at zero energy level after convergence. $\dot{V}_1(t) = 0$ shows that controller (33) takes 2 s to keep the closed-loop at zero after convergence but oscillates in the steady state. $\dot{V}_2(t) = 0$ demonstrates that the closed-loop will not reach zero as the energy gradient function becomes zero before the convergence; it shows that the controller (34) is not successfully bringing the system's synchronization error energy to zero. Therefore, the control signals shown in Figure 11(c) are ineffective in attaining zero synchronization error energy function. In this case, the control signal energy develops sustained oscillations in the synchronization error states.

The inequality (35) and the simulation results in Figure 13(a and b) illustrate that the proposed RDASCS (17) furnishes faster convergence than the other two controllers as the energy dissipation initial rate is high. In the vicinity of zero, the energy dissipation rate is low. This characteristic improved closed-loop stability, reduced computation time, and increased synchronization accuracy.

7. Conclusions

This paper discusses the chaotic behaviour of a financial system using theoretical analysis and numerical simulations. Then, it proposes a novel adaptive control algorithm for synchronizing two identical four-dimensional chaotic financial systems supported by a detailed stability analysis of the designed closed-loop. The computer simulation results and theoretical analysis show that the proposed adaptive controller achieves faster and smoother synchronization error convergence to the origin for the unknown time-varying model with uncertainties and exogenous disturbances. The Lyapunov second stability theorem guarantees the closed-loop's robust performance against bounded time-varying unknown exogenous disturbances and un-modelled dynamics. The article also includes theoretical and computer simulation analysis demonstrating that the designed closed-loop behaviour is lesser oscillatory and that control effort is chatter-free and smoother than the other state-of-the-art controllers selected for the comparative study. The proposed robust synchronization control of two identical hyperchaotic finance systems can be beneficial in improving the security, stability, prediction, performance, and flexibility of financial systems.

Timely buffeting-free synchronization can improve financial systems' behaviour. Therefore, pre-assigned settling time and buffeting suppression synchronization algorithms should be developed in future. The proposed article can provide a paradigm for the analysis.

Disclosure statement

No potential conflict of interest was reported by the author(s).

ORCID

Israr Ahmad http://orcid.org/0000-0002-3053-1158

References

[1] Strogatz SH. Nonlinear dynamics and chaos, with applications to physics, biology, chemistry, and engineering. Reading (MA): Addison-Wesley; 1994.
[2] Jun-hai MS, Yu-shu C. Study of the bifurcation topological structure and the global complicated character of a kind of nonlinear finance system (II). Appl Math Mech. 2001;22(11):1240–1251. doi:10.1007/BF02437847
[3] Jian JG, Deng XL, Wang JF. Globally exponentially attractive set and synchronization of a class of chaotic finance system. Lecture Notes Comput Sci. 2009;5551:253–261. doi:10.1007/978-3-642-01507-6_30
[4] Gao Q, Ma J. Chaos and Hopf bifurcation of a finance system. Nonlinear Dyn. 2009;58:209–216. doi:10.1007/s11071-009-9472-5
[5] Chian ACL, Rempel ER, Rogers C. Complex economic dynamics: chaotic saddle, crisis and intermittency. Chaos Solit Fract. 2006;29:1194–1218. doi:10.1016/j.chaos.2005.08.218

[6] Haojie Y, Guoliang C, Yuxiu L. Dynamic analysis and control of a new hyperchaotic finance system. Nonlinear Dyn. 2012;67:2171–2182. doi:10.1007/s11071-011-0137-9
[7] Zhao X, Li Z, Li S. Synchronization of chaotic finance system. Appl Math Comput. 2011;217:6031–6039.
[8] Chai X, Gan Z, Shi C. Impulsive synchronization and adaptive-impulsive synchronization of a novel financial hyperchaotic system. Math Prob Engin. 2013;Article ID 751616:10.
[9] Vargas JAR, Grzeidak E. Robust adaptive synchronization of a hyperchaotic finance system. Nonlinear Dyn. 2014;80(1–2):239–248.
[10] Xu YH, Xie CR, Wang YL, et al. Chaos projective synchronization of the chaotic finance system with parameter switching perturbation and input time-varying delay. Math Meth App Sci. 2014;38(17):4279–4288. doi:10.1002/mma.3364
[11] Ding K, Xu X. Mixed synchronization of chaotic financial systems by using linear feedback control. Discrete Dyn Nature Soc. 2016;Article ID 3269248:7.
[12] Jajarmi A, Hajipur M, Baleanu D. New aspects of the adaptive synchronization and hyperchaos suppression of a financial model. Chaos Solit Fract. 2017;99:285–296. doi:10.1016/j.chaos.2017.04.025
[13] Tirandaz H, Aminabadi SS, Tavakoli H. Chaos synchronization and parameter identification of a finance chaotic system with unknown parameters, a linear feedback controller. Alexandria Engin J. 2018;57:1519–1524. doi:10.1016/j.aej.2017.03.041
[14] Lu L, Wei Q. Parameter estimation and synchronization in the uncertain financial network. Physica A. 2019;53:122418. doi:10.1016/j.physa.2019.122418
[15] Chen H, Yu L, Wang Y, et al. Synchronization of a hyperchaotic finance system. Complexity. 2021;Article ID 6618435):7. doi:10.1155/2021/6618435
[16] Onma OS, Heryanto, Foster B, et al. Adaptive control and multi-variables projective synchronization of hyperchaotic finance system. 2021 IOP Conf Ser Mater Sci Eng. 2021;1115:012003. doi:10.1088/1757-899X/1115/1/012003
[17] Shi W, Ding Y, Cai G. Synchronization analysis of a new hyperchaotic finance system model via linear feedback control. 33rd Chinese Cont Decis Conf (CCDC); 2021, Kunming, People's Republic of China.
[18] Wang C, Zhao X, Zhang Y, et al. Global existence and fixed-time synchronization of a hyperchaotic financial system governed by semi-linear parabolic partial differential equations equipped with the homogeneous neumann boundary condition. Entropy. 2023;25:359. doi:10.3390/e25020359
[19] Wei J, Zhao D, Liang L. Estimating the growth models of news stories on disasters. J AM Soc Inf Sci Technol. 2009;60(9):1741–1755. doi:10.1002/asi.21109
[20] Zhao M, Wang J. $\boldsymbol{H}_\infty$ control of a chaotic finance system in the presence of external disturbance and input time-delay. App Math Comput. 2014;233:320–327. doi:10.1016/j.amc.2013.12.085
[21] Khalil HK. Nonlinear system. 2nd ed. Upper Saddle River (NJ): Prentice-Hall; 2002.
[22] Khan A, Kumar S. Measuring chaos and synchronization of chaotic satellite systems using sliding mode control. Optimal Control App Meth. 2018;39(5):1597–1609. doi:10.1002/oca.2428
[23] Grebogi C, Ott E, Yorke JA. Chaos, strange attractors, and fractal basin boundaries in nonlinear dynamics. Science. 1987;238(4827):632–638. doi:10.1126/science.238.4827.632
[24] Greiner W. Lyapunov exponents and chaos. In: Classical mechanics. 2nd ed. Heidelberg, Berlin: Springer; 2010. p. 503–516.
[25] Guckenheimer J, Holmes P. Nonlinear oscillations, dynamical systems, and bifurcation of vector fields. 3rd ed. New York: Springer-Verlag; 1997.
[26] Aghababa MP, Heydari A. Chaos synchronization between two different chaotic systems with uncertainties, external disturbances, unknown parameters and input nonlinearities. App Math Model. 2012;36(4):1639–1652. doi:10.1016/j.apm.2011.09.023
[27] Fang JS, Tsaim JSH, Yan JJ, et al. Adaptive chattering-free sliding mode control of chaotic systems with unknown input nonlinearity via smooth hyperbolic tangent function. Math Prob Engin. 2019; Article ID 4509674:9.
[28] Aghababa MP, Akbari ME. A chattering-free robust adaptive sliding mode controller for synchronization of two different chaotic systems with unknown uncertainties and external disturbances. Appl Math Comput. 2012;218(9):5757–5768.
[29] Haris M, Shafiq M, Ahmad I, et al. Nonlinear feedback controller for the synchronization of hyper(chaotic) systems with known parameters. J Math Comp Sci. 2020;23:124–135. doi:10.22436/jmcs.023.02.05
[30] Shinners SM. Modern control system theory and design. New York: John Wiley and Sons; 1998.